NEURAL REGENERATION RESEARCH
www.nrronline.org

Research Article

Neuroinflammatory responses and synaptic impairment in a Herpes simplex virus type 1 model of sporadic Alzheimer's disease

Domenica Donatella Li Puma[1, 2, *], Giammarco Boni[1], Giulia Puliatti[1], Bruno Bandiera[1], Marco Rinaudo[1, 2], Francesco Lerose[2], Giovanna De Chiara[3], Anna Teresa Palamara[4, 5], Roberto Piacentini[1, 2, *], Claudio Grassi[1, 2]

https://doi.org/10.4103/NRR.NRR-D-25-01175

Date of submission: August 8, 2025

Date of decision: November 1, 2025

Date of acceptance: November 11, 2025

Date of web publication: April 14, 2026

From the Contents

Graphical Abstract

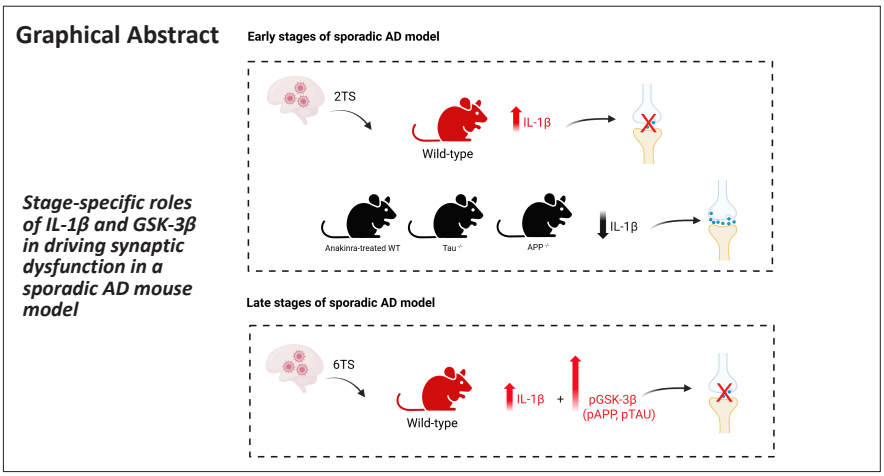

Abstract

Alzheimer's disease is a progressive neurodegenerative disorder in which neuroinflammation has emerged as a key contributor to early synaptic and cognitive dysfunction. In previous studies, we demonstrated that the spread of herpes simplex virus type 1 infection to the central nervous system and its reactivation induced by thermal stress, triggers the accumulation of Alzheimer's disease molecular hallmarks and the development of an Alzheimer's disease-like phenotype in wild-type C57BL/6 mice. In particular, two cycles of thermal stress–induced reactivation in wild-type mice induced a marked upregulation of the proinflammatory cytokine interleukin-1β, along with hippocampal synaptic and memory deficits, features reminiscent of an early stage of neurodegeneration. Notably, blocking interleukin-1β signaling with anakinra, a pharmacological interleukin-1 receptor antagonist, fully rescued all structural and functional indices of neurodegeneration, highlighting the central role of neuroinflammation in early phases of the disease. Here, we documented that, in addition to increased interleukin-1β levels, two cycles of thermal stress promoted the activation of glycogen synthase kinase 3β through phosphorylation of the tyrosine residue at position 216 (Tyr216), along with elevated phosphorylation of its direct substrates, amyloid precursor protein (APP) at threonine 668 and tau at Serine 199. To dissect the contribution of APP and tau to herpes simplex virus type 1-induced synaptic dysfunction, we employed $APP^{-/-}$ and $Tau^{-/-}$ mice. After two cycles of thermal stress, these knock-out mouse models exhibited lower increases in interleukin-1β levels and smaller synaptic deficits than infected wild-type mice, along with a distinct profile of microglial activation. To determine whether neuroinflammation remains the predominant pathological driver at later stages, we extended our analyses to herpes simplex virus type 1-infected wild-type mice subjected to six cycles of thermal stress (6TS), which recapitulate an advanced disease stage with features reminiscent of an Alzheimer's disease-like phenotype. Although interleukin-1β levels remained persistently elevated in mice subjected to six cycles of thermal stress, anti-inflammatory treatments with either anakinra or dexamethasone failed to rescue synaptic and memory deficits, suggesting that neuroinflammation was no longer the primary pathological driver. Instead, synaptic failure correlated with a pronounced increase in glycogen synthase kinase 3β-induced APP cleavage products (e.g., amyloid-β) and hyperphosphorylated tau, indicating a stage-dependent shift in pathogenic mechanisms, whereby early neuroinflammatory responses are progressively replaced by other processes primarily mediated by glycogen synthase kinase 3β. These findings underscore the stage-specific contribution of interleukin-1β and glycogen synthase kinase 3β to herpes simplex virus type 1-induced Alzheimer's disease-like synaptic failure, highlighting the importance of a phase-specific therapeutic strategy.

Key Words: amyloid precursor protein; amyloid-β; anakinra; dexamethasone; glycogen synthase kinase 3β; herpes simplex virus type 1; interleukin-1β; memory; synaptic plasticity; Tau

Introduction

Alzheimer's disease (AD) is the most common neurodegenerative disorder, characterized by insidious onset, progressive behavioral alterations, and cognitive decline. Extensive preclinical and clinical evidence has identified amyloid-β (Aβ) and tau as key players in AD pathophysiology due to their accumulation in insoluble aggregates and soluble oligomeric forms (Spires-Jones and Hyman, 2014; Pradeepkiran et al., 2024), the latter being considered primarily responsible for early synaptic failure (Selkoe, 2002). In the past decade, increasing evidence has revealed elevated levels of inflammatory markers in postmortem brain tissue from AD patients and has identified several AD-associated risk genes involved in innate immune processes (Sudwarts and Thinakaran, 2023; Sun et al., 2023; Heneka et al., 2025). These discoveries strongly support the view that neuroinflammation is a major determinant of AD pathophysiology, playing a critical role in cognitive impairment (Leng and Edison, 2021). This chronic inflammatory response is largely orchestrated by microglial cells that become persistently activated in AD (Ebrahimi et al., 2025; Valiukas et al., 2025). Once activated, microglia undergo dynamic phenotypic changes in response to microenvironmental cues, adopting transcriptional states promoting the sustained release of proinflammatory cytokines (Isik et al., 2023).

[1]Department of Neuroscience, Università Cattolica del Sacro Cuore, Rome, Italy; [2]Fondazione Policlinico Universitario A. Gemelli IRCCS, Rome, Italy; [3]Institute of Translational Pharmacology, National Research Council (CNR), Rome, Italy; [4]Department of Infectious Diseases, Istituto Superiore di Sanità, Rome, Italy; [5]Department of Public Health and Infectious Diseases, Sapienza University of Rome, Laboratory Affiliated to Istituto Pasteur Italia-Cenci Bolognetti Foundation, Rome, Italy
***Correspondence to:** Roberto Piacentini, PhD, roberto.piacentini@unicatt.it; Domenica Donatella Li Puma, PhD, domenicadonatella.lipuma@unicatt.it.
https://orcid.org/0000-0003-4215-1643 (Roberto Piacentini); https://orcid.org/0000-0001-6729-6967 (Domenica Donatella Li Puma)

Funding: *This study was supported by the National Recovery and Resilience Plan (NRRP), Mission 4, Component 2, Investment 1.1, Call for tender No. 104 published on 02/02/2022 and 1409 published on 09/14/2022 by the Italian Ministry of University and Research (MUR), funded by the European Union – NextGenerationEU– Project 2022ZYLB7B – CUP J53D23010129000 8 and B53D23003770006 - Grant Assignment Decree No. D.D. 104, 02/02/2022 (to GDC and CG) and Project P2022YW7BP – CUP J53D23016130001 (Grant Assignment Decree No D.D. 1223 07/31/2023 to CG); and financial support from Italian Ministry of Health: Ricerca Corrente 2025, Fondazione Policlinico Universitario A. Gemelli IRCCS (to CG).*
How to cite this article: *Li Puma DD, Boni G, Puliatti G, Bandiera B, Rinaudo M, Lerose F, De Chiara G, Palamara AT, Piacentini R, Grassi C (2026) Neuroinflammatory responses and synaptic impairment in a Herpes simplex virus type 1 model of sporadic Alzheimer's disease. Neural Regen Res 21(11):5632-5641.*

Highlights

- Demonstrates that synaptic dysfunction induced by recurrent HSV-1 reactivations is mediated by IL-1β-dependent neuroinflammation in the early phases, whereas later stages involve GSK-3β-dependent tau/Aβ accumulation.
- Confirms the essential role of APP and tau in sustaining IL-1β-mediated neuroinflammation across C57BL/6, APP$^{-/-}$, and tau$^{-/-}$ mice in the early stages of neurodegeneration.
- Shows that anti-inflammatory strategies restore molecular and cognitive functions only at early disease stages but become ineffective at later stages.
- Identifies GSK-3β/tau signaling as a late and druggable pathway beyond inflammation, supporting targeted and stage-specific therapeutic strategies for HSV-1–associated Alzheimer-like pathology.

This cascade ultimately contributes to synaptic and neuronal degeneration (Gao et al., 2023; Zhang et al., 2023).

To gain insights into the molecular mechanisms leading to synaptic dysfunction in AD, and to identify the relative contribution of neuroinflammation vs. molecular hallmarks such as Aβ and/or hyperphosphorylated tau forms (pTau) to this effect, we exploited the mouse model of recurrent herpes simplex virus type-1 (HSV-1) infection already described in De Chiara et al., 2019 and further characterized in Li Puma et al., 2021 and 2023. In this model, repeated reactivations of the virus into the brain, reminiscent of what can occur in HSV-1-infected humans throughout life, determine a time-dependent neuroinflammation, as documented by astrogliosis and increased levels of interleukins, along with the occurrence and accumulation of classical AD hallmarks such as Aβ and pTau. Epidemiological and clinical studies have consistently linked HSV-1 reactivation with increased risk of cognitive decline and AD (Lövheim et al., 2015; Vestin et al., 2024; Araya et al., 2025; Liu et al., 2025), thereby supporting the rationale for using this model to explore stage-dependent mechanisms of neurodegeneration.

Here, we aim to dissect the relative contribution of neuroinflammation and AD hallmarks to the synaptic dysfunction exhibited by this sporadic model of AD during the progression of the disease. Based on our previous findings (Li Puma et al., 2023), we hypothesize that the proinflammatory cytokine interleukin-1β (IL-1β)-mediated neuroinflammation predominates at early stages, whereas at later stages, synaptic dysfunction is increasingly sustained by glycogen synthase kinase 3β (GSK-3β)-mediated amyloid precursor protein (APP) cleavage products (e.g., Aβ peptides) or phosphorylated tau. Indeed, GSK-3β activation occurs either through increased phosphorylation at Tyr216 or through reduced inhibitory phosphorylation at Ser9 (Zhou et al., 2022; Yu et al., 2023), and we previously demonstrated that this kinase is a key determinant of HSV-1–induced synaptic dysfunction *in vitro* (Piacentini et al., 2015). We further aim to define the specific contribution of APP and tau to the IL-1β-mediated neuroinflammatory response in the early stages of disease. These insights have potential therapeutic implications, underscoring the need for phase-specific treatment strategies for AD.

Methods

Animals

Adult male wild-type (C57BL/6) mice, APP Knockout (B6.129S7-Apptm1Dbo/J; APP$^{-/-}$), and tau Knockout (B6.129X1-Mapttm1Hnd/J; Tau$^{-/-}$) mice purchased from The Jackson Laboratory were used for this work. Colonies were maintained at the animal facility of Università Cattolica del Sacro Cuore, Rome. Mice were housed under controlled environmental conditions, with constant humidity (50%) and temperature (21 ± 1°C), on a 12-hour light/dark cycle, with *ad libitum* access to food and water. All animal procedures were approved by the Ethics Committee of Università Cattolica (authorizations No. 916/2020-PR and No. 271/2024-PR) and were fully compliant with the Italian (Ministry of Health guidelines, Legislative Decree No. 116/1992) and European Union (Directive No. 86/609/EEC) legislation on animal research.

In vivo mouse model of recurrent herpes simplex virus type 1 infection

A mouse model of recurrent HSV-1 brain infection was established in male C57BL/6 and transgenic APP$^{-/-}$ and Tau$^{-/-}$ mice, as previously described (De Chiara et al., 2019; Li Puma et al., 2019, 2023). One-month-old mice were inoculated via lip scarification with either HSV-1 (F strain, 1 × 10^6 plaque-forming units in 2 µL) or vehicle (2 µL). Six weeks later, when viral latency was likely established, mice underwent thermal stress (TS; 40–42°C for 15 minutes) to induce viral reactivation and brain spread. TS was applied monthly, and animals were analyzed 1 week after the second (at 4.5 months of age) or sixth reactivation (at 7.5 months of age).

Animals subjected to behavioral testing (novel object recognition [NOR], *n* = 19–32 per group at 2TS; *n* = 12–26 per group at 6TS) represented the primary cohort. Subsets of these animals were subsequently employed for electrophysiological analysis (long-term potentiation [LTP] recordings, *n* = 6–9 per group at 2TS; *n* = 5–7 per group at 6TS). Additional subsets from the same behavioral cohorts were used for molecular studies. Whole brains were dissected; one hemisphere (A) was assigned to Western blot (*n* = 4–7 per group) or quantitative reverse transcription-polymerase chain reaction (qRT-PCR; *n* = 4–7 per group at 2TS; *n* = 5–6 per group at 6TS) and the contralateral hemisphere (B) to the other assays (dot blot [*n* = 4] or enzyme-linked immunosorbent assay [ELISA; *n* = 4–5]). Immunohistochemistry (*n* = 5 at 2TS) was performed on fixed brains sacrificed following behavioral tests (*n* = 5 at 2TS). RNA-seq was conducted in independent cohorts (*n* = 3 per group) using fresh brain tissue, with no overlap with behavioral-electrophysiological-molecular readouts. **Additional Table 1** summarizes sample sizes, ages, and tissue/hemisphere allocation, and indicates if the same animals/tissues were used across the different assays.

Pharmacological treatments

To assess the contribution of neuroinflammation in HSV-1-induced synaptic alterations, both mock- and HSV-1-infected mice received intraperitoneal injections of anakinra (30 mg/kg; IL-1R blocker; Kineret®, Sobi, Stockholm, Sweden) or dexamethasone (5 mg/kg; Sigma, St. Louis, MO, USA) for 3 consecutive days: the day before TS (D_{-1}), the day of TS (D_0), and the day after TS (D_1). To investigate the involvement of GSK-3β, mice were treated with lithium chloride (LiCl, 45 mg/kg, intraperitoneally) every other day for 3 weeks after 5TS (Li et al., 2023).

Immunocytochemistry and image analysis

Hippocampal slices were processed for immunofluorescence as previously described in Li Puma et al. (2019). After fixation in 4% paraformaldehyde, slices were treated with Triton X-100 (Sigma; 0.3% in PBS) for 15 minutes to allow membrane permeabilization. Cells were then incubated for 20 minutes with 0.3% bovine serum albumin in PBS to block nonspecific binding sites and then incubated overnight at 4°C with rabbit anti-$Aβ_{40–42}$ (1:300, Cat# AB5076, Millipore, Bedford, MA, USA) and mouse anti-neuronal nuclei (NeuN; 1:500, Cat# AB5076, Millipore). The next day, slices were incubated for 90 minutes at room temperature (25°C, room temperature) with the appropriate secondary antibodies from Thermo Fisher Scientific, Waltham, MA, USA, all used at a dilution of 1:1000 in PBS: Alexa Fluor-488 donkey anti-rabbit (Cat# A21206); Alexa Fluor-546 donkey anti-mouse (Cat# A10036). Cell nuclei were counterstained with 4',6-diamidino-2-phenylindole (DAPI; 0.5 µg/mL; Cat# D1306, Thermo Fisher Scientific), and the cells were finally coverslipped with ProLong Gold antifade reagent (Thermo Fisher Scientific).

Confocal stacks of images were acquired at 60× magnification with a confocal laser scanning system (A1MP, Nikon, Tokyo, Japan) and an oil-immersion objective (N.A. 1.4). Immunoreactivity for $Aβ_{40/42}$ was quantified by drawing regions of interest around neurons (NeuN-positive) in the CA1 and CA3 areas in the acquired field. The $Aβ_{40/42}$ load was calculated as the product of the percentage of $Aβ_{40/42}$-positive cells and the mean signal intensity in those cells..

Novel object recognition test

Recognition memory was assessed using the novel object recognition (NOR) test, following the procedures described by Akkerman et al. (2012). On the first day, the animals were familiarized for 10 minutes with the test arena (45 cm × 45 cm). On the second day (training session), they were allowed to explore two identical objects placed symmetrically in the arena for 10 minutes. On the third day (test session), a new object replaced one of the old objects. Animals were allowed to explore for 10 minutes, and a preference index (PI), calculated as the ratio between the time spent exploring the novel object and the time spent exploring both objects, was used to measure recognition memory. Animal behavior was manually analyzed in blind by an experienced user through the tracking software ANY-maze™ (Stoelting). Briefly, exploratory behavior was manually analyzed in blind by an experienced user and defined as the snout pointing toward the object at a maximum distance of 2 cm. Climbing or touching the object with the forepaws or tail without the head directed toward it was not considered exploration.

Electrophysiological recordings

Extracellular field recordings were conducted on 400 µm-thick hippocampal coronal slices as previously described (Li Puma et al., 2023). Slices were placed in a recording chamber and perfused (2–3 mL/min) with artificial cerebrospinal fluid containing (in mM) 124 NaCl, 2,5 KCl, 1,25 Na_2HPO_4, 25 $NaHCO_3$, 2 $CaCl_2$, 1 $MgCl_2$, and 11 glucose, maintained at 29°C, and continuously bubbled with 95% O_2 and 5% CO_2. After 120 minutes of recovery, field excitatory postsynaptic potentials (fEPSPs) were recorded in the CA1 stratum radiatum using a glass electrode filled with artificial cerebrospinal fluid in response to Schaffer collateral stimulation by a bipolar tungsten electrode. First, the input-output relationship was constructed, and the stimulation intensity that elicited one-third of the maximal response was used to deliver test pulses every 20 seconds. After achieving a stable baseline response, LTP was induced using the high-frequency stimulation (HFS) protocol (one train of stimuli at 100 Hz, lasting 500 ms, repeated four times with an inter-train interval of 20 seconds). LTP magnitude was expressed as the percentage change in the mean fEPSP peak amplitude normalized to the baseline values (i.e., mean values for the last 5 minutes of recording before high-frequency stimulation). Recordings were performed in the current clamp I=0 mode using a Multiclamp 700B/Digidata 1440 A system (Molecular Devices, San Jose, CA, USA).

Western blotting and dot blot analyses

Hippocampal and cortical murine tissues isolated from C57BL/6, APP$^{-/-}$ and Tau$^{-/-}$ mice were lysed in ice-cold lysis buffer (NaCl 150 mM, Tris-HCl 50 mM pH 8, and ethylenediaminetetraacetic acid 2 mM) containing 1% Triton X-100, 0.1% sodium dodecyl sulfate (SDS), 1× protease inhibitor cocktail (Sigma), 1 mM sodium orthovanadate (Sigma), and 1 mM sodium fluoride (Sigma). Equal amounts of protein were diluted in Laemmli buffer, boiled, and resolved by SDS-polyacrylamide gel electrophoresis as previously described (Li Puma et al., 2019, 2022; Colussi et al., 2023; Puliatti et al., 2023). For the

dot blot, 4.5 µL of hippocampal lysates (30 µg/µL) were spotted onto a nitrocellulose membrane and stained with Ponceau S. Membranes were blocked with 5% non-fat dry milk in tris-buffered saline containing 0.1% Tween-20 for 1 hour at room temperature and then incubated overnight at 4°C with the following primary antibodies (all diluted 1:1000): mouse anti-phosphorylated GSK-3β (pGSK-3β) Tyr216 (Cat# 05-413, Merck, Darmstadt, Germany), rabbit anti-GSK-3β (Cat# D5C5Z, Cell Signaling Technology, Danvers, MA, USA), rabbit anti-phosphorylated APP (pAPP) threonine 668 (Thr668; Cat# 6986, Cell Signaling Technology), rabbit anti-APP (Cat# 76600, Cell Signaling Technology), rabbit anti-IL-1β (Cat# sc-7884, Santa Cruz Biotecnology, Dallas, TX, USA), rabbit anti-ionized calcium-binding adaptor molecule 1 (Iba1; Cat# 17198, Cell Signaling Technology), rabbit anti-CD86 (Cat# AB-84415, Immunological Sciences, Rome, Italy); rabbit anti- NOD-, LRR- and pyrin domain-containing protein 3 (NLRP3; Cat# MA5-23919, Thermo Fisher Scientific, Waltham, MA, USA); mouse anti-synaptophysin (SYP; Cat# ab8049, Abcam, Cambridge, UK), mouse anti-AMPA receptor subunit GluA1 (Cat# MAB2263, Merck), mouse anti-glyceraldehyde 3-phosphate dehydrogenase (Cat# ab9484, Abcam), rabbit anti β-actin (Cat# ab8227, Abcam), rabbit anti-α-/β-tubulin (Cat# 2146S, Cell Signaling Technology); rabbit anti-APP intracellular domain (AICD; Cat# 811901, BioLegend, San Diego, CA, USA). Protein expression was quantified using UVItec Cambridge Alliance. Molecular weights were identified using Precision Plus Protein Dual Color Standards (Bio-Rad, Hercules, CA, USA). Data were calculated by normalizing densitometry values to the mean of the control condition (mock=1). Changes in expression were reported as "fold induction" relative to the control. Western blot (WB) experiments were performed in four independent replicates.

Enzyme-linked immunosorbent assay

The concentrations of murine $A\beta_{42}$ and phosphorylated Tau (pTau S199) were determined using the following ELISA kits, according to the manufacturers' instructions: mouse amyloid beta 42 ELISA kit (Cat# KMB3441, Thermo Fisher Scientific); mouse Tau (Phospho) [pS199] ELISA kit (Cat# KMB7041, Thermo Fisher Scientific). Protein levels measured by ELISA were normalized to the mean of the control condition (mock=1). Expression changes were reported as "fold induction" relative to the control.

Quantitative reverse transcription-polymerase chain reaction

qRT-PCR amplifications were performed as described in (Li Puma et al., 2019, 2023) using specific primers (**Table 1**) and the Power SYBRTM Green PCR Master Mix (Applied Biosystems, Foster City, CA, USA) on AB7500 instrument. Samples were run in triplicate and relative mRNA levels for genes of interest were normalized to glyceraldehyde 3-phosphate dehydrogenase and calculated using the $2^{-\Delta\Delta Ct}$ method.

Table 1 | **Primer sequences used for quantitative reverse transcription-polymerase chain reaction analysis**

Gene	Primer sequence (5'–3')
IL-1β	F: CTG TGA CTC ATG GGA TGA TGA TG
	R: GCC TGT AGT GCA GTT GTC TAA T
Iba1	F: CTT GAA GCG AAT GCT GGA GAA
	R: GGC AGC TCG GAG ATA GCT TT
GAPDH	F: TGC CAA GTA TGA TGA CAT CAA GAA G
	R: GGT CCT CAG TGT AGC CCA AGA

F: Forward; GAPDH: glyceraldehyde 3-phosphate dehydrogenase; Iba1: ionized calcium-binding adaptor molecule 1; IL-1β: interleukin-1β; R: reverse.

Digital mRNA sequencing

Mouse hippocampal tissue (n = 3 mice per group) from mock- and HSV-1-infected mice (both WT and transgenic) was used for RNA extraction, library preparation, RNA sequencing, and data analysis, all performed by NEGEDIA S.r.l., Pozzuoli (NA), Italy. Specifically, total RNA was quantified using the Qubit 4.0 fluorimetric assay (Thermo Fisher Scientific). Libraries were prepared from 125 ng of total RNA using the NEGEDIA S.r.l. Digital mRNA-seq research grade sequencing service v2.0, which included library preparation, quality assessment, and sequencing on a NovaSeq 6000 sequencing system using a single-end, 100-cycle strategy (Illumina Inc., San Diego, CA, USA).

Differentially expressed genes (DEGs) were identified using a P-value ≤ 0.05 and fold-change above 1.5 (calculated as a mean ratio between treated and non-treated samples). Microglia-related genes that were differentially expressed in our models were analyzed for pathway enrichment using the Enrichr database, and the results are reported in **Additional Table 2**. Specifically, we considered microglial genes that were up- or down-regulated in the AD mouse model (Holtman et al., 2015) as well as genes induced by Aβ and tau (Gan et al., 2004; Udeochu et al., 2023), and on microglial gene modules (type 1 and type 2) derived from mouse brain datasets (Miller et al., 2010). Gene identifiers were mapped to Entrez IDs using the biomaRt package (v2.65.16; Benner et al., 2014) to ensure a perfect match between the expression dataset and the microglia gene-set (Smedley et al., 2009). The reference genome used was mm10.

Gene Ontology enrichment analysis

Gene Ontology (GO) enrichment analysis was performed to identify significant biological processes among DEGs. The analysis was conducted in R (version 4.5.1; Xu et al., 2024) using the clusterProfiler package (v4.17.0) and the org.Mm.eg.db annotation database (v3.21.0). The bar plots were generated by using ggplot2 package in R (v 4.0.0; Wickham, 2016).

Gene visualization

Heatmaps were generated in R using the pheatmap package (version 1.0.13), applying row-wise scaling and complete linkage for hierarchical clustering. A heatmap for each group comparison was reported. The overlap between the DEG lists of each group comparison and custom microglia-related pathways was visualized with ggplot2 package in R (version 4.0.0).

Statistical analysis

Statistical significance was assessed using appropriate statistical analyses based on the type of comparison performed. Data normality and homogeneity of variance between groups were verified using the Shapiro-Wilk test prior to analysis. The specific statistical tests used (i.e., Student's t-test, Mann-Whitney U test, Kruskal-Wallis one-way analysis of variance on ranks, one- or two-way analysis of variance, followed by Student-Newman-Keuls *post hoc* test) are indicated in the corresponding figure legends for each experiment. The number of animals (n) in each experiment is specified in the figure legends and in **Additional Table 3**. Data are presented as mean ± SEM. Statistical significance was set at $P < 0.05$. Analyses were performed using SigmaPlot 14.0 software (Systat Software Inc., San Jose, CA, USA). The effect size (Cohen's d for two-group comparisons, Cohen's f for multiple-group comparisons) was calculated using G*Power version 3.1.9.7 (Heinrich Heine University Düsseldorf, Düsseldorf, Germany) assuming a statistical power of at least 0.80.

Results

Herpes simplex virus type 1 infection in C57BL/6 mice triggers glycogen synthase kinase 3β phosphorylation at Tyr216, leading to increased levels of the amyloid precursor protein-derived fragments and phosphorylated Tau

We recently demonstrated that, after 2TS, HSV-1-infected C57BL/6 mice exhibited increased levels of IL-1β, negatively affecting synaptic function, thus leading to memory deficits. The causal role of IL-1β in these effects was validated using the IL-1R blocker anakinra, which fully rescued the structural and functional indices of neurodegeneration (Li Puma et al., 2023). Here, we documented that 2TS also triggered the activation of GSK-3β at the hippocampal level through phosphorylation at Tyr216, in infected mice, compared with mock-infected ones (1.46 ± 0.08 *vs.* 1.00 ± 0.15, P = 0.029, d = 2.47; **Figure 1A** and **B**). As such, we found an increased phosphorylation of GSK-3β substrates in infected mice compared with mock-infected ones (set to 1): APP at Thr668, 1.71 ± 0.12 *vs.* 1.00 ± 0.23; P = 0.008, d = 2.09; **Figure 1A** and **C**) and tau at Serine 199 (Ser199; 1.33 ± 0.12 *vs.* 1.00 ± 0.08, P = 0.029, d = 2.23; **Figure 1D**), a well-validated and direct GSK-3β target (Foidl and Humpel, 2018). Similar results were also obtained at the cortical level (**Additional Table 4**).

APP phosphorylation represents a crucial event for its proteolytic cleavage (Hampel et al., 2021). Since the Thr668 residue is located in the C-terminal region of APP, its phosphorylation, besides promoting amyloidogenic processing leading to Aβ formation, also contributes to the non-amyloidogenic pathway with the production of the non-toxic fragment P3 along with increased production and nuclear accumulation of AICD, a fragment that is known to modulate gene transcription (Bórquez and González-Billault, 2012; Ng et al., 2024). Consistent with our previous *in vitro* data (Civitelli et al., 2015), we showed that mice subjected to 2TS exhibited a significant increase in AICD production at the hippocampal level compared with control mice (1.72 ± 0.18 *vs.* 1.00 ± 0.12, P = 0.029, d = 2.47; **Figure 1E** and **F**), confirming our previous findings that HSV-1 enhances APP processing (De Chiara et al., 2010). In agreement with these results, confocal microscopy analysis revealed that neurons of the CA1 and CA3 regions of the hippocampus of infected mice at 2TS exhibited a significant increase in $A\beta_{40/42}$ load with respect to mock-infected mice. In particular, the percentage of cells exhibiting a detectable accumulation of $A\beta_{40/42}$ rose from 13.5% in mock-infected mice to 55.4% in HSV-1-infected ones. Also, the signal intensity in Aβ40/42-positive cells increased in infected mice even if, in this case, the increment was moderate (+12%). Therefore, to obtain an overall quantification of $A\beta_{40/42}$ load in the hippocampi of HSV-1–infected mice, we calculated the "$A\beta_{40/42}$ load" by multiplying the percentage of $A\beta_{40/42}$-positive cells by the mean $A\beta_{40/42}$ signal intensity within those cells. Then, by setting equal to 1.00 ± 0.06 the value in mock-infected hippocampi, this increased by ten-fold in HSV-1-infected ones (to 9.65 ± 0.14; P = 0.045; **Additional Figure 1A–E**).

However, ELISA performed on hippocampal lysates from HSV-1-infected C57BL/6 mice subjected to 2TS did not show such an increase relative to control mice (set to 1), showing a modest and not statistically significant Aβ accumulation (1.25 ± 0.17 *vs.* 1.00 ± 0.11, P = 0.174, d = 2.09; **Additional Figure 1F**). We hypothesize that this discrepancy most likely arises from the use of total hippocampal homogenates including cells not accumulating $A\beta_{40/42}$, and may therefore mask the increases observed in HSV-1–infected CA1/CA3 neurons. Altogether, these findings indicate that 2TS-induced HSV-1 reactivation triggers GSK-3β activation and promotes the accumulation of its downstream substrates.

Amyloid precursor protein and tau deletion mitigates herpes simplex virus type 1-induced synaptic dysfunction

We hypothesized that APP processing and tau phosphorylation play a role in the synaptic dysfunction induced by HSV-1 infection. Hyperphosphorylated tau has long been recognized as a pathological hallmark of AD, contributing to synaptic loss and neuronal damage in the brain (Gu and Liu, 2020; Rawat et al., 2022; Gonzalez-Ortiz et al., 2023). Similarly, APP generates the toxic fragment Aβ and AICD and facilitates the intercellular

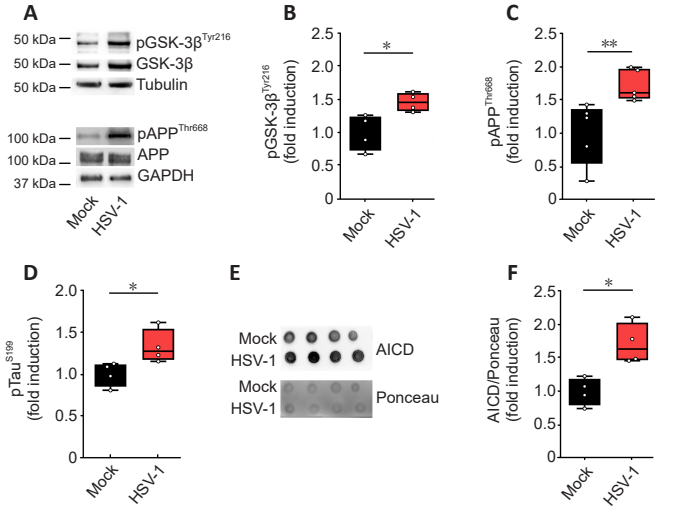

Figure 1 | **HSV-1 reactivation promotes the phosphorylation of GSK-3β at Tyr216 and its substrates APP at Thr668 and tau at Ser199.**

(A–C) Representative Western blot images (A) and densitometric analyses of pGSK-3β^{Tyr216} (B) and pAPP^{Thr668} (C) protein levels in hippocampal lysates from mock- and HSV-1-infected mice (n = 4 for both) sacrificed after two cycles of thermal stress. Tubulin and GAPDH were used as loading controls. (D) Box plot showing pTau^{S199} levels in hippocampal homogenates from mock- and HSV-1-infected mice (n = 5 mice) quantified by enzyme-linked immunosorbent assay. Values are expressed as fold changes relative to controls (set as 1). (E, F) Representative dot blot images (E) and quantification (F) showing increased AICD protein levels in hippocampal lysates from HSV-1-infected mice compared with controls (n = 4 mice per group). Ponceau staining confirmed equal protein loading.*P < 0.05, **P < 0.01 (Mann-Whitney U test). AICD: APP intracellular domain; APP: amyloid precursor protein; GAPDH: glyceraldehyde 3-phosphate dehydrogenase; GSK-3β: glycogen synthase kinase 3β; HSV-1: herpes simplex virus type 1; n.s., not significant; pAPP: phosphorylated APP; pGSK-3β: phosphorylated GSK-3β.

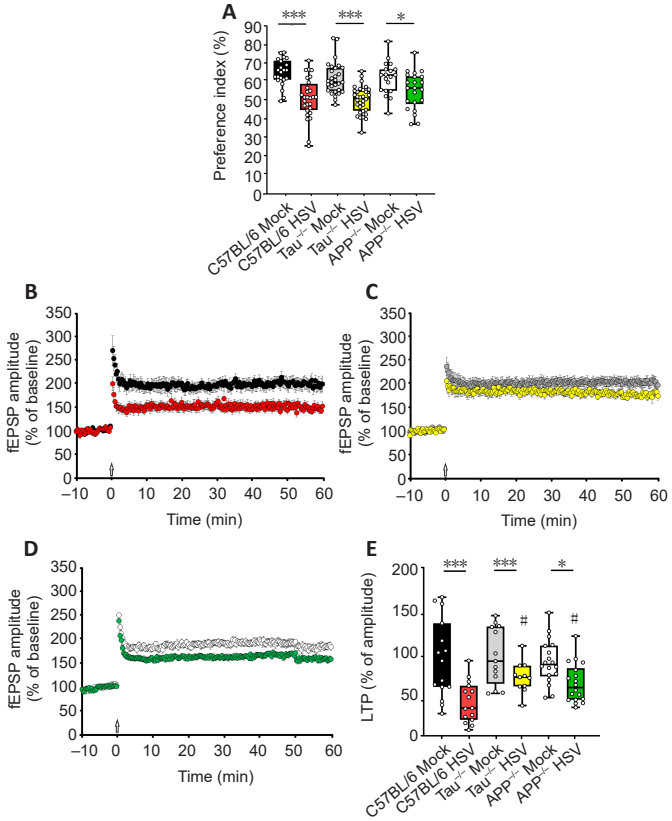

Figure 2 | **HSV-1-infected Tau$^{-/-}$ and APP$^{-/-}$ mice subjected to 2TS exhibit impaired recognition memory and milder long-term potentiation improvements than infected wild-type mice.**

(A) Box plot showing the mean preference index for the novel object in the novel object recognition test performed after the 2nd thermal stress in C57BL/6 (n = 22 mock, n = 28 HSV-1), Tau$^{-/-}$ (n = 29 mock, n = 32 HSV-1) and APP$^{-/-}$ mice (n = 19 mock, n = 22 HSV-1). (B–D) Mean time course of field excitatory postsynaptic potential amplitude before and after high-frequency stimulation (indicated by the arrow) in hippocampal slices from mock- and HSV-1-infected (B) wild-type mice (mock: n = 15 slices from 6 mice; HSV-1: n = 15 slices from 6 mice), (C) Tau$^{-/-}$ mice (mock: n = 13 slices from 6 mice; HSV-1: n = 11 slices from 9 mice), and (D) APP$^{-/-}$ mice (mock: n = 18 slices from 8 mice; HSV-1: n = 18 slices from 6 mice). (E) Box plot showing the mean long-term potentiation during the last 5 minutes of recording in control and infected groups. *P < 0.05, ***P < 0.001; #P < 0.05, $vs.$ C57BL/6 HSV-1-infected mice (two-way analysis of variance followed by Student-Newman-Keuls $post\ hoc$ test). APP: Amyloid precursor protein; fEPSP: field excitatory postsynaptic potential; HSV-1: herpes simplex virus type 1.

spreading of tau and Aβ oligomers (Multhaup et al., 2015; Puzzo et al., 2017; Li Puma et al., 2022; Puliatti et al., 2023). Based on this evidence, we investigated the specific contributions of APP and tau to HSV-1-induced synaptic dysfunction by using genetically modified mice lacking either APP or tau expression (APP$^{-/-}$ and Tau$^{-/-}$). We first assessed cognitive performance in 4.5-month-old mice using the NOR test, which evaluates recognition memory by exploiting the natural tendency of animals to explore novel stimuli. We found that mock-infected mice of all strains (both WT and transgenic) were able to distinguish between familiar and novel objects, and no significant differences were observed in the PI among the groups (p = 0.35, f = 0.38; **Additional Figure 2A**). In contrast, all the HSV-1-infected mice undergone 2TS showed impaired recognition memory, spending similar amounts of time exploring both the familiar and the novel objects during the test phase. Specifically, the PI values in HSV-1-infected $vs.$ mock-infected mice were: 50.7 ± 1.3% $vs.$ 62.0 ± 1.6% in Tau$^{-/-}$ mice, P < 0.001; 55.7 ± 2.2% $vs.$ 62.5 ± 2.1% in APP$^{-/-}$ mice, P = 0.015; and 51.6 ± 2.1% $vs.$ 65.2 ± 1.6% in WT mice (P < 0.001, f = 0.29; **Figure 2A**). To gain insights into the detrimental effects of HSV-1 infection on memory, we studied LTP at the CA3-CA1 hippocampal synapse, which is considered the cellular correlate of learning and memory (Bliss and Collingridge, 1993). Field excitatory postsynaptic potential recordings (**Additional Figure 2B**) showed no significant differences in LTP (**Additional Figure 2C**) among the mock-infected mouse genotypes (WT, APP$^{-/-}$, and Tau$^{-/-}$, P = 0.87; f = 0.47), consistent with the memory performance results. However, field potential recording (**Figure 2B–D**) showed that the impairment in synaptic potentiation caused by 2TS-induced reactivations of HSV-1 in the brain was milder in mice lacking tau (76.6 ± 5.8% $vs.$ 101.5 ± 9.8% of mock, P = 0.046; **Figure 2C** and **E**) and APP (69.5 ± 5.6% $vs.$ 94.6 ± 6.4% of mock; P = 0.014, **Figure 2D** and **E**) compared with WT mice (47.3 ± 6.4 $vs.$ 98.0 ± 12.4; P < 0.001; **Figure 2B** and **E**; f = 0.39). Thus, the loss of APP or tau partially preserved synaptic plasticity following HSV-1 reactivation, in contrast to the pronounced deficits observed in WT mice.

Herpes simplex virus type 1-infected APP$^{-/-}$ and Tau$^{-/-}$ mice exhibit reduced interleukin-1β expression

Since the deletion of either APP or tau only partially spared mice from the synaptic deficits induced by HSV-1 infection and reactivation and in light of our previous evidence identifying IL-1β as a key player in synaptic damage of infected mice, we investigated the contribution of IL-1β to the synaptic deficits observed in the transgenic mice. As a first step, we assessed IL-1β mRNA levels in both mock- and HSV-1-infected mice after 2TS. While no differences were found among the three mock-infected strains (P = 0.83, f = 0.91; **Figure 3A**), indicating that the absence of APP or tau did not affect basal IL-1β mRNA expression, significant differences were observed between HSV-1-infected WT and transgenic mice after 2TS. Indeed, in line with our recent findings (Li Puma et al., 2023), qRT-PCR revealed a significant increase in IL-1β expression in HSV-1-infected WT mice compared with mock-infected mice (2.43 ± 0.36-fold, P = 0.006, d = 2.03; **Figure 3B**), but this increase was attenuated in both HSV-1-infected Tau$^{-/-}$ and APP$^{-/-}$ mice (1.65 ± 0.28-fold, P = 0.048, d = 1.87, and 1.39 ± 0.08-fold, respectively, P = 0.001, d = 1.76, respectively, compared with their respective controls; **Figure 3B**). Thus, although HSV-1 infection increased IL-1β levels in both knockout models, this upregulation was significantly lower than in HSV-1-infected WT mice: –34%, P = 0.005 in Tau$^{-/-}$ mice and –45%, P = 0.011 in APP$^{-/-}$ mice (f = 0.73; **Figure 3B**). The reduction in $IL\text{-}1\beta$ mRNA levels was also reflected at the protein level. Indeed, WB analysis performed on hippocampal lysates from HSV-1-infected mice (**Figure 3C**) revealed that the amount of IL-1β produced following HSV-1 infection was lower in Tau$^{-/-}$ and APP$^{-/-}$ mice than in C57BL/6 mice (from 3.37 ± 0.96 to 1.47 ± 0.53 and 1.49 ± 0.60, P = 0.031 and P = 0.013, respectively; f = 0.73, **Figure 3D**).

A large body of evidence indicates that the maturation and subsequent release of the pro-inflammatory cytokine IL-1β are tightly regulated by the activation of the NLRP3 inflammasome, a cytosolic multiprotein complex that activates inflammatory caspase-1, which in turn cleaves inactive pro-IL-1β to produce its biologically active form (Blevins et al., 2022; Liang et al., 2022; Chen et al., 2023; Li et al., 2024; Ye et al., 2024). Therefore, we wondered whether the different levels of IL-1β we found in the three mouse strains might result from genotype-specific variations in NLRP3 inflammasome activation following HSV-1 infection. The basal NLRP3 expression (i.e., in the absence of infection), evaluated by WB analysis (**Additional Figure 3A**), did not significantly differ among the groups (P = 0.47, f = 0.81; **Additional Figure 3B**), and no statistically significant differences were observed in upregulation of NLRP3 protein across all infected genotypes following 2TS compared with their respective mock controls. Specifically, NLRP3 levels increased to 1.72 ± 0.34 $vs.$ 1.00 ± 0.11, P = 0.048 in WT mice, 1.68 ± 0.24 $vs.$ 1.00 ± 0.18, P = 0.048 in Tau$^{-/-}$ mice and 1.92 ± 0.28 $vs.$ 1.00 ± 0.24, P = 0.030, in APP$^{-/-}$ mice (d = 1.87 for both conditions). Notably, no significant differences were detected among the infected genotypes (P = 0.12; f = 0.81), thus suggesting that the different upregulation of IL-1β levels upon HSV-1 infection did not depend on different inflammasome activation among the three genotypes.

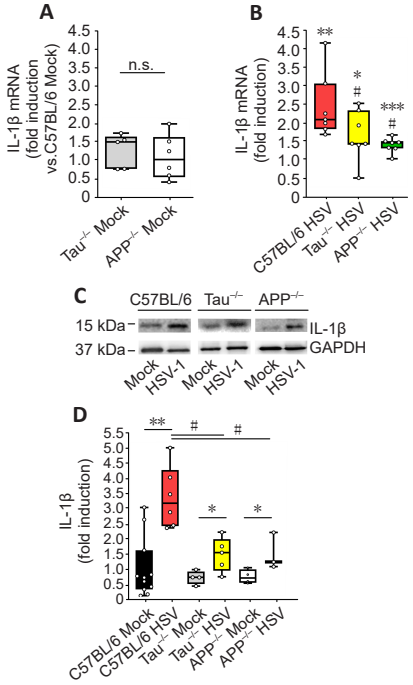

Figure 3 | IL-1β expression in HSV-1- infected Tau$^{-/-}$ and APP$^{-/-}$ mice is lower than in infected WT mice.

Relative mRNA expression levels of *IL-1β* analyzed in uninfected control mice (Tau$^{-/-}$ n = 5, APP$^{-/-}$ n = 6) respect to C57BL/6 mice (n = 4) (A) and HSV-1-infected mouse strains after 2 thermal stress-TS (n = 7 per strain) (B) compared with their respective controls; (C) Representative western blot (WB) analysis of activated IL-1β protein levels in hippocampal tissue collected from mice 24 hours after 2TS (n = 4 mice per group). GAPDH was used as a loading control. (D) Densitometric quantification from three independent WB experiments performed as shown in C normalized to C57BL/6 mice. *P < 0.05, **P < 0.01, ***P < 0.001; #P < 0.005, *vs.* C57BL/6 HSV-1-infected mice (Kruskal-Wallis one-way analysis of variance on ranks). APP: Amyloid precursor protein; GAPDH: glyceraldehyde 3-phosphate dehydrogenase; HSV-1: herpes simplex virus type 1; IL-1β: interleukin-1β; n.s.: not significant.

Herpes simplex virus type 1-infected APP$^{-/-}$ and Tau$^{-/-}$ mice exhibit altered microglial activation

We then checked whether the reduced IL-1β production observed in the absence of either APP or tau resulted from a different microglial response to HSV-1 infection. We began by examining the expression of Iba1, which is a general marker of microglial activation. No differences were observed in *Iba1* levels between mock-infected mouse strains, either at the mRNA level (P = 0.21, f=1.07; **Figure 4A**) or at the protein level, evaluated by WB analysis (P = 0.33, f = 1.00; **Figure 4C**). Following HSV-1 infection, increased *Iba1* levels were observed both at the mRNA level (1.48 ± 0.27-fold in C57BL/6 mice, P = 0.016, d=2.27; 1.34±0.09-fold in Tau$^{-/-}$ mice, P = 0.029, d = 2.47; and 1.66 ± 0.16-fold in APP$^{-/-}$ mice, P = 0.016, d = 2.27 compared with mock-infected mice; **Figure 4B**) and at the protein level (1.82 ± 0.14 *vs.* 1.00 ± 0.20, P = 0.016, d = 2.27; 2.07 ± 0.12 *vs.* 1.00 ± 0.14, P = 0.029, d = 2.45; and 1.95 ± 0.23 *vs.* 1.00 ± 0.16, P = 0.029, d = 2.47, in HSV-1-infected C57BL/6, Tau$^{-/-}$, and APP$^{-/-}$ mice, respectively, compared with mock-infected mice set to 1; **Figure 4C** and **D**). However, Iba1 is a pan-microglial marker that did not allow us to distinguish between resting and activated microglia. Therefore, we analyzed the expressions of microglial activation markers, including CD86, which is a marker commonly upregulated in M1-like pro-inflammatory microglia that promotes the production of cytokines such as IL-1β (Jurga et al., 2020; Xu et al., 2022; Lee and Chang, 2025). CD86 protein levels were significantly upregulated in HSV-1-infected mice compared with mock-infected mice (set to 1): 2.60 ± 0.51 *vs.* 1.00 ± 0.09, d = 2.27; 1.47 ± 0.18 *vs.* 1.00 ± 0.02, d = 2.47; and 1.37 ± 0.10 *vs.* 1.00 ± 0.09, d = 2.47 in C57BL/6, Tau$^{-/-}$, and APP$^{-/-}$ mice, respectively; p = 0.029 for all (**Figure 4E**, **F**). Notably, CD86 upregulation in HSV-1-infected transgenic mice was significantly lower than in infected WT mice (–43% in Tau$^{-/-}$, p = 0.004; –47% in APP$^{-/-}$, p = 0.04, f = 1.07). The attenuated CD86 response observed in APP$^{-/-}$ and Tau$^{-/-}$ mice is consistent with the reduced IL-1β production detected in these genotypes, supporting a role for APP and tau in sustaining a pro-inflammatory microglial phenotype.

To further assess genotype dependence of the previous results, we performed an exploratory RNA-seq analysis to test the hypothesis that genotype-specific transcriptional programs, particularly those related to synaptic function and microglial activation, underlie the divergent responses between WT and transgenic mice. Among 19470 genes analyzed, HSV-1 infection significantly modulated 682 transcripts in WT (**Additional Figure 4A**), 460 in Tau$^{-/-}$ (**Additional Figure 4B**), and 685 in APP$^{-/-}$ mice (**Additional Figure 4C**). The heatmaps show the expression profiles of significantly deregulated genes across the analyzed groups. Distinct clustering patterns were observed for each

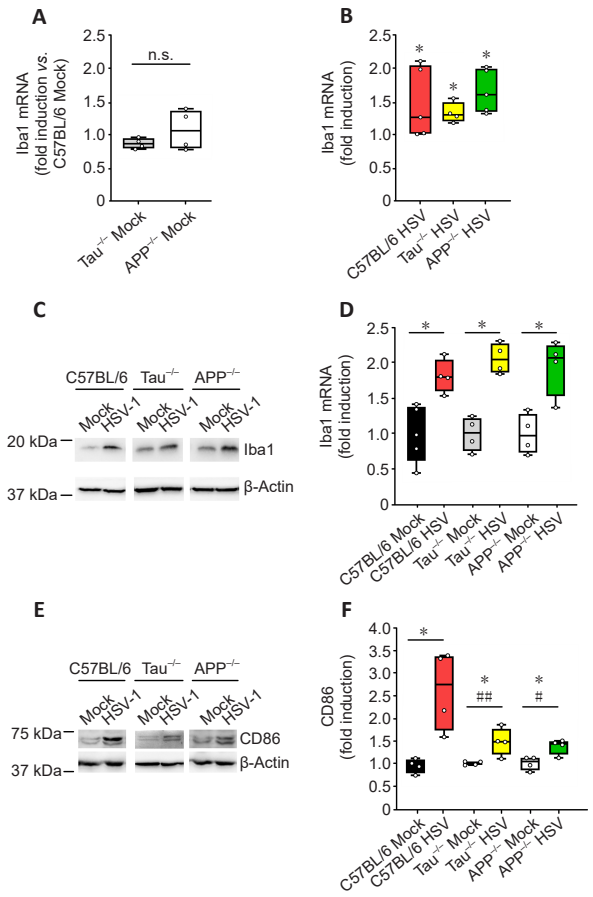

Figure 4 | HSV-1-infected Tau$^{-/-}$ and APP$^{-/-}$ mice exhibit altered M1-type microglial activation compared with wild-type mice after two cycles of thermal stress.

(A, B) Box plots showing *Iba1* mRNA levels in wild-type, Tau$^{-/-}$ and APP$^{-/-}$ mice under mock and HSV-1 conditions (n = 4/5 per group). (C, D) Representative western blot images (C) and quantification (D) of Iba1 protein levels in mock- (n = 4/5 mice) and HSV-1-infected mice (n = 4 for all mouse strains). (E, F) CD86 protein expression in mock- (n = 4/5 mice) and HSV-1-infected mice (n = 4 for all mouse strains) analyzed after 2 thermal stress. *P < 0.05, *vs.* mock; #P < 0.05, ##P < 0.01, *vs.* C57BL/6 HSV-1-infected mice, assessed by Kruskal-Wallis one-way analysis of variance on ranks or Mann-Whitney *U* test. APP: Amyloid precursor protein; HSV-1: herpes simplex virus type 1; Iba1: ionized calcium-binding adaptor molecule 1; n.s.: not significant.

specific group comparison, indicating group-specific transcriptional signatures. We thus investigated whether the modulated genes were enriched in pathways related to synaptic function (e.g., synapse assembly, synaptic vesicle recycling). GO analysis indicates that the same synaptic pathways were enriched across strains and, although the leading-edge genes underlying that enrichment differed by genotype, some of them were going in the same direction (upregulation).

Among the modulated DEGs in C57BL/6 HSV-1-infected *versus* mock-infected mice, the enriched biological processes (BP) included post-synapse organization, regulation of postsynaptic membrane neurotransmitter receptor levels, regulation of synapse structure or activity, regulation of synapse organization, vesicle-mediated transport in synapses, synapse assembly, and BP associated with translation at the pre-synapse and post-synapse (**Additional Figure 4A1** and **A2**).

In Tau$^{-/-}$ mice, we found enrichment in protein localization to synapse, regulation of postsynaptic membrane neurotransmitter receptor levels, protein localization to the post-synapse, and synapse assembly and processes related to neuron migration (**Additional Figure 4B1** and **B2**), and finally, in APP$^{-/-}$ mice, the upregulated BP were associated with regulation of synapse organization, synapse assembly, the synaptic vesicle cycle and regenerative processes (**Additional Figure 4C1** and **C2**).

These data could indicate that each genotype activates distinct subprocesses within the same pathways, contributing to strain-specific modulation of synaptic function.

To identify the microglial gene component, we intersected each DEGs set with a curated list of microglia-specific genes (see Methods and **Additional Table 2**). This yielded 110 out of 682 genes in WT, 79/460 in Tau$^{-/-}$, and 102/685 in APP$^{-/-}$ mice (**Figure 5A–C**). Transcriptomic analysis revealed that HSV-1-infected C57BL/6 mice exhibited increased expression of several genes associated with microglial activation (**Figure 5A** and **A1**), consistent with a previous study in murine models of AD (Holtman et al., 2015). For instance: *Nav1*, a gene encoding a subtype of voltage-gated sodium channels, that was

identified as a direct target of tau (Udeochu et al., 2023) and is involved in the functional responses of activated microglia (Black et al., 2009); *Ets2*, modulated by both Aβ and tau, and acting as a key mediator of the inflammatory response through the induction of genes encoding pro-inflammatory cytokines, chemokines, and other inflammatory mediators (Ben-Aicha and Ramos, 2025). Besides the previously mentioned upregulated genes, other genes were found significantly downregulated (**Figure 5A** and **A2**), yet in line with observations in AD models (Holtman et al., 2015). Among them, we identified *Tspan14*, which controls ADAM10 maturation and, in turn, drives the ectodomain shedding of TREM2 to yield sTREM2, a process implicated in AD-related microglial signaling (Yang et al., 2023), and *Tmem18*, whose DNA methylation is associated with neuritic amyloid plaque burden (He et al., 2022).

Finally, we also observed that several genes, i.e., *Fabp5*, *Spp1*, *Higd1a*, *Npm1*, and *Susd6*, which are typically upregulated in AD models, were downregulated in our model (**Figure 5A** and **A3**). Given that these genes are known to be induced by Aβ (Gan et al., 2004), the lack of their induction might be attributed to the low Aβ levels detected, which could impair their transcriptional regulation.

Notably, in the transgenic KO models (APP and Tau), the very few genes shared across genotypes do not recapitulate the known AD-like patterns (Holtman et al., 2015), in terms of both up/down regulation and effect magnitude (**Figure 5B–C3**). In these mouse models, we observed a significant modulation of other genes, which may activate alternative molecular pathways that are beyond the scope of our study, through which microglia exert their functions.

These data suggest that based on microglia activation, our model recapitulates an AD-like phenotype and that both APP and tau are required to trigger this microglial activation, leading to the AD phenotype, likely following different pathways.

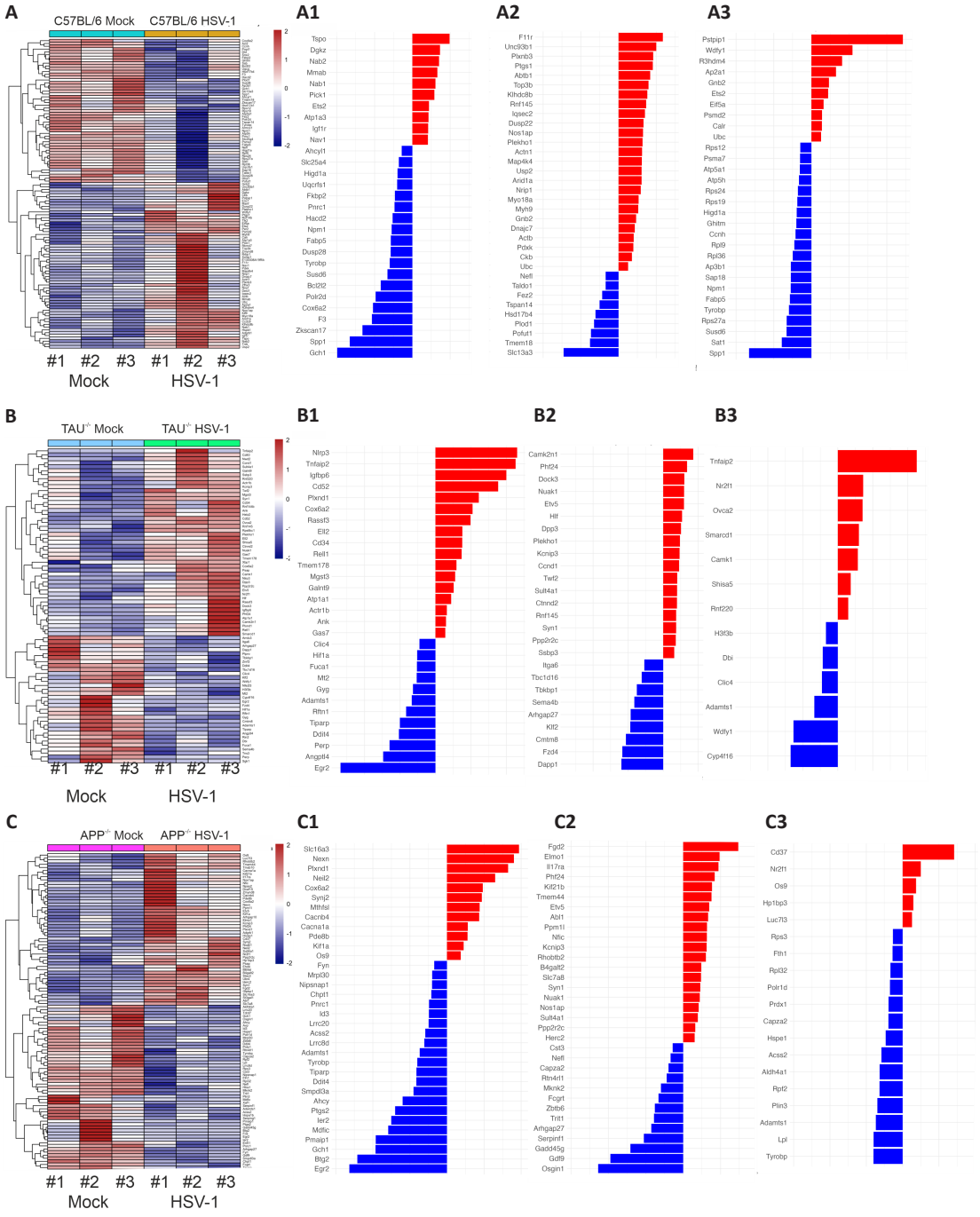

Figure 5 | Modulation of Alzheimer's disease-related microglial genes across the three genotypes following HSV-1 infection.
(A–C) Heatmaps of microglia-specific differentially expressed genes in (A) wilt-type (n = 110/682 DEGs), (B) Tau$^{-/-}$ (n = 79/460), and (C) APP$^{-/-}$ (n = 102/685) comparing mock-infected and HSV-1–infected conditions; rows are genes; columns are individual samples (mock on the left, HSV-1–treated on the right); values are row-wise z-scores of normalized expression; genes are ordered by unsupervised hierarchical clustering; the color scale denotes higher (red) and lower (blue) expression relative to each gene's mean. The corresponding bar plots display expression levels of microglia-specific differentially expressed genes that are (A1, B1, C1) enriched in genes upregulated in Alzheimer's disease mouse models, (A2, B2, C2) enriched in genes downregulated in Alzheimer's disease mouse models, and (A3, B3, C3) enriched in genes induced by amyloid-β exposure. APP: Amyloid precursor protein; HSV-1: herpes simplex virus type 1.

C57BL/6 mice undergoing multiple herpes simplex virus type 1 reactivations still exhibit synaptic and memory dysfunction

The findings described so far indicate that, after 2TS, the major determinant of the synaptic dysfunction is the pro-inflammatory cytokine IL-1β, whose upregulation following HSV-1 infection nicely correlates with microglial activation and synaptic deficits in the different studied genotypes. Based on these results, we investigated whether inflammation remained the primary driver of pathology in the later stages of the disease. To address this issue, we used an HSV-1-infection WT model subjected to repeated viral reactivations (6TS), which is reminiscent of overt AD phenotype (De Chiara et al., 2019). First, we characterized the effects of repeated HSV-1 reactivation on hippocampus-dependent memory and synaptic function. The results of the NOR paradigm revealed a marked impairment of hippocampus-mediated cognitive functions in HSV-1-infected mice subjected to the 6TS, as demonstrated by a significant reduction in the PI for the novel object compared with mock-infected animals (51.9% ± 1.2% *vs.* 64.9% ± 2.0%, $P < 0.001$, $f = 0.29$; **Figure 6A**). To gain insights into the detrimental effects of HSV-1 infection on memory, we studied LTP at the CA3-CA1 hippocampal synapse. In brain slices from mock-infected mice, the fEPSP amplitude (**Figure 6B**) recorded 60 minutes after high-frequency stimulation was 103.7% ± 16.7% greater than the baseline. However, in slices from HSV-1-infected mice subjected to 6TS, this increase was significantly lower than that of mock-infected mice (56.5% ± 6.3%; $P = 0.003$; $f = 0.48$; **Figure 6C**).

To explore the molecular basis of the synaptic and cognitive impairments observed after 6TS, we analyzed changes in the expression of some key proteins involved in synaptic plasticity following recurrent HSV-1 reactivation, such as SYP (a presynaptic vesicle protein) and the AMPA receptor subunit GluA1 (crucial for excitatory transmission and LTP). In infected mice, WB analysis carried out on hippocampal samples revealed a marked reduction in SYP (0.30 ± 0.06 *vs.* 1.00 ± 0.04, $P = 0.036$, $f = 0.83$; **Figure 6D** and **E**) and GluA1 (0.30 ± 0.03 *vs.* 1.00 ± 0.14, $P = 0.028$, $f = 0.81$; **Figure 6D** and **F**) compared with control mice (set to 1). These two proteins were specifically chosen as representative markers of presynaptic and postsynaptic integrity, respectively, and their downregulation provides a plausible molecular basis for the impaired hippocampal plasticity and memory performance observed in HSV-1–infected mice after 6TS. In summary, repeated HSV-1 reactivations (6TS) in C57BL/6 mice cause robust deficits in hippocampus-dependent memory and LTP, accompanied by reduced SYP and GluA1 expression.

Anti-inflammatory treatments fail to reverse synaptic and cognitive deficits in HSV-1–infected wild-type mice after six cycles of thermal stress

The next step was to investigate whether the synaptic and cognitive deficits observed at 6TS still depended on increased IL-1β expression. To address this issue, we first quantified IL-1β levels in hippocampal tissue from both mock- and HSV-1-infected mice exposed to the 6TS paradigm. As expected, *IL-1β* levels were significantly increased in infected mice compared with controls, both at the mRNA (2.17 ± 0.65-fold induction, $P = 0.006$; $d = 2.27$; **Additional Figure 5A**) and at the protein levels (2.21 ± 0.52 *vs.* 1.00 ± 0.91, $P = 0.020$; $d = 1.80$; **Additional Figure 5B** and **C**). Notably, IL-1β does not increase further from 2TS to 6TS ($P = 0.108$, $f = 0.74$), indicating no significant stage-dependent change of neuroinflammatory status. However, in contrast to what we observed at the second viral reactivation, at 6TS, the IL-1R blocker anakinra (30 mg/kg, i.p) administered following the scheme outlined in **Additional Figure 6** did not spare HSV-1-infected mice from functional and molecular synaptic dysfunction. These mice displayed indeed a significant impairment of cognitive performances assessed by the NOR paradigm. Specifically, they exhibited a marked deficit in their ability to discriminate between familiar and novel objects, as evidenced by a PI of 52.5% ± 2.6% that was significantly lower than that of anakinra-treated mock-infected mice (65.6% ± 1.7%; $P < 0.001$, $f = 0.29$; **Figure 7A**), which did not display any impairment.

Behavioral impairment in anakinra-treated HSV-1-infected mice was paralleled by functional deficits in synaptic plasticity. Specifically, following LTP induction, the fEPSP amplitude potentiation in HSV-1-infected mice treated with anakinra was significantly lower than that observed in mock-infected mice subjected to the same IL-1R blockade (66.4% ± 6.1% *vs.* 99.6% ± 11.6%; $P = 0.041$, $f = 0.48$; **Figure 7B** and **C**). Accordingly, the expression of both pre- and postsynaptic proteins in the hippocampi of anakinra-treated and infected mice was downregulated (0.31 ± 0.09 *vs.* 1.00 ± 0.14 for SYP and 0.27 ± 0.13 *vs.* 0.94 ± 0.18 for GluA1, $P = 0.041$, $f = 0.83$ and $P = 0.044$, $f = 0.81$, respectively, *vs.* treated mock-infected mice; **Figure 7D–F**). These results suggest that the IL-1β blockade is no longer effective at this disease stage and the increased IL-1β levels observed in 6TS mice is not the primary determinant of synaptic dysfunction observed in mice subjected to multiple viral reactivations. To better understand the role of neuroinflammation in our experimental model and the contribution of other pro-inflammatory cytokines, we treated mice with dexamethasone, a potent corticosteroid that is known to enhance the transcription of anti-inflammatory cytokines while repressing the transcription of pro-inflammatory cytokines (Joyce et al., 1996; Strickland et al., 2022). C57BL/6 mice received dexamethasone (5 mg/kg, i.p., Shishkina et al., 2023), as described in **Additional Figure 6** and were analyzed after 2TS and 6TS. After 2TS, dexamethasone treatment reverted synaptic dysfunction induced by HSV-1, mirroring the beneficial effects previously reported for anakinra on LTP (Li Puma et al., 2023). Specifically, no significant differences in LTP, evaluated in terms of field excitatory postsynaptic potential recordings (**Figure 8A**) were observed between dexamethasone-treated HSV-1-infected and mock-infected mice (77.6% ± 7.3% *vs.* 86.3% ± 11.3%, respectively; $P = 0.5$, $f = 0.45$;

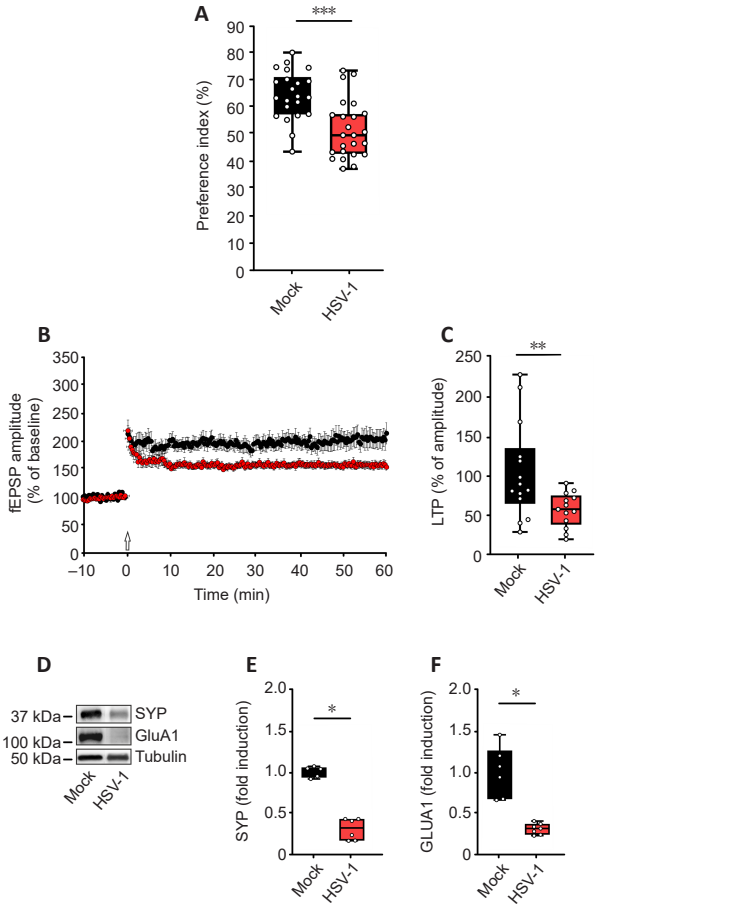

Figure 6 | **Altered cognitive and synaptic function in mice subjected to six cycles of thermal stress.**

(A) Box plot showing the mean value of preference index in the novel object recognition paradigm for mock and HSV-1-infected C57BL/6 mice ($n = 22$ and $n = 24$ mice, respectively). (B) Mean time course of field excitatory post-synaptic potential amplitude before and after high-frequency stimulation (indicated by arrow) in hippocampal slices from: mock- ($n = 15$ slices from 6 mice) and HSV-1- infected-C57BL/6 mice ($n = 13$ slices from 5 mice). (C) Box plot comparing long-term potentiation amplitudes measured during the last 5 minutes of recording in controls and infected mice. (D) Representative western blot images of pre- and post-synaptic proteins in hippocampal lysates from mock- and HSV-1-infected mice. (E, F) Box plots showing the densitometric analysis of synaptophysin (SYP) and GluA1 in mock- ($n = 5$ and $n = 6$, respectively) and HSV-1-infected mice ($n = 6$ and $n = 7$). $^*P < 0.05$, $^{**}P < 0.01$, $^{***}P < 0.001$ (two-way analysis of variance followed by Student-Newman-Keuls *post hoc* test [A–C], Kruskal-Wallis one-way analysis of variance on ranks [E, F]). fEPSP: Field excitatory postsynaptic potential; GluA1: AMPA receptor subunit; HSV-1: herpes simplex virus type 1; LTP: long-term potentiation; SYP: synaptophysin.

Figure 8B). The improvement in LTP following dexamethasone treatment was statistically significant compared with untreated HSV-1-infected mice (77.6% ± 7.3% *vs.* 47.3% ± 6.4%, respectively; $P = 0.029$, $f = 0.45$). However, as previously observed with anakinra, after 6TS dexamethasone failed to rescue the synaptic plasticity deficits induced by virus infection and reactivation, with LTP values of 58.3% ± 6.2% in HSV-1-infected mice compared with 90.1% ± 6.7% in treated mock-infected mice ($P = 0.028$, $f = 0.46$; **Figure 8C** and **D**). These results suggest that, although an inflammatory response persists at later stages of the phenotype, it is not the main driver of the observed synaptic deficits.

In light of these findings, we shifted our focus to investigate whether repeated viral reactivations lead to increased activation of GSK-3β, resulting in enhanced production and accumulation of APP cleavage products (e.g., Aβ) and/or pTau, which may contribute to the anti-inflammatory treatment-resistant synaptic dysfunction observed in the later stages of HSV-1–induced disease. The active form of GSK-3β, induced by phosphorylation at Tyr216, was increased to 2.94 ± 0.24 *vs.* 1.00 ± 0.09 ($P = 0.012$; $d = 2.47$) in infected animals at 6TS, compared with 1.46 ± 0.08 at 2TS ($P = 0.02$; $f = 0.97$) as shown by WB analysis reported in **Figure 9A** and the relative quantification reported in **Figure 9B**. Accordingly, a significant increase in $pTau^{Ser199}$ and Aβ levels was observed in the hippocampal tissue of 6TS HSV-1-infected mice. ELISA measurements revealed that $pTau^{Ser199}$ levels were elevated to 1.72 ± 0.04 *vs.* 1.00 ± 0.04 and Aβ levels were elevated to 2.02 ± 0.09 *vs.* 1.00 ± 0.09 ($P = 0.016$ and $P = 0.012$, respectively). These increases were significantly higher with respect to the values observed in infected animals after 2TS

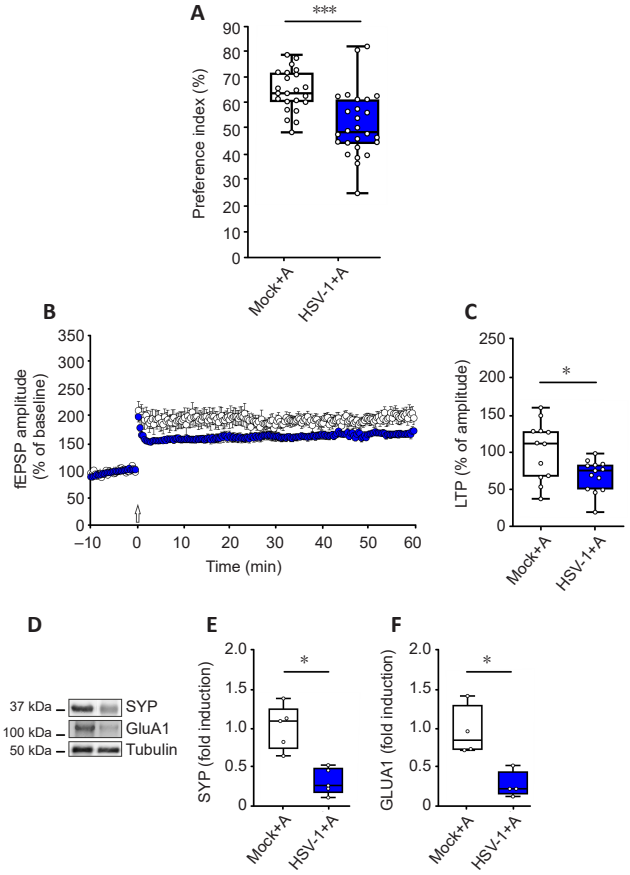

Figure 7 | **Anakinra fails to rescue synaptic and memory impairments in mice undergoing six cycles of thermal stress.**
(A) Box plot showing the mean value of preference index in the novel object recognition paradigm for mock and HSV-1-infected C57BL/6 mice treated with anakinra (mock+A [*n* = 23 mice] and HSV-1+A [*n* = 26 mice]). (B) Mean time course of field excitatory post-synaptic potential amplitude before and after high-frequency stimulation (indicated by arrow) in hippocampal slices from mice treated with anakinra (mock+A [*n* = 12 slices from 5 mice] and HSV-1+A [*n* = 13 slices from 5 mice]). (C) Box plot comparing long-term potentiation amplitudes measured during the last 5 minutes of recording in controls and infected mice. (D) Representative immunoblots of pre- and post-synaptic proteins in hippocampal lysates from mock- and HSV-1-infected mice treated with anakinra. (E, F) Box plots showing the densitometric analysis of SYP and GluA1 in anakinra-treated mock- (*n* = 5 and *n* = 4) and infected mice (*n* = 5 and *n* = 4). **P* < 0.05, ****P* < 0.001 (two-way analysis of variance followed by Student-Newman-Keuls *post-hoc* test [A–C], Kruskal-Wallis one-way analysis of variance on ranks [E, F]). fEPSP: Field excitatory postsynaptic potential; GluA1: AMPA receptor subunit; HSV-1: herpes simplex virus type 1; LTP: long-term potentiation; SYP: synaptophysin.

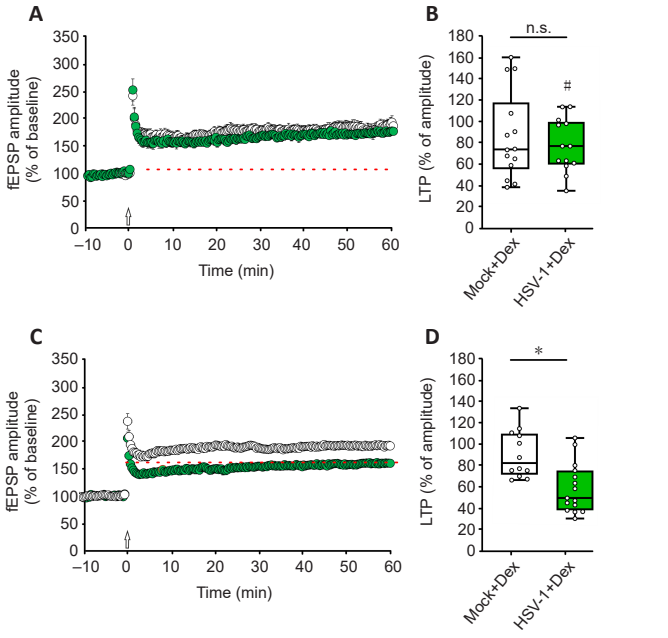

Figure 8 | **Dexamethasone rescues HSV-1-induced synaptic deficits in mice subjected to two cycles of thermal stress, but is ineffective following six cycles of thermal stress.**
(A, C) Mean time course of field excitatory postsynaptic potential amplitude before and after high-frequency stimulation (indicated by arrow) in hippocampal slices from: (A) mice treated with dexamethasone (mock+dex [*n* = 14 slices from 5 mice] and HSV-1+dex [*n* = 13 slices from 5 mice]) and analyzed 1 week after two cycles of thermal stress; (C) mice treated with dexamethasone (mock+dex [*n* = 13 slices from 5 mice] and HSV-1+dex [*n* = 15 slices from 6 mice]) and sacrificed 1 week after six cycles of thermal stress. (B, D) Bar graphs showing mean long-term potentiation in the last 5 minutes of recording in controls and infected mice. The red dotted lines indicate the mean values of long-term potentiation observed in untreated HSV-1-infected C57BL/6 mice. **P* < 0.05; #*P* < 0.05 *vs.* HSV-1, assessed by two-way analysis of variance followed by Student-Newman-Keuls *post hoc* test. fEPSP: Field excitatory postsynaptic potential; HSV-1: herpes simplex virus type 1; LTP: long-term potentiation; n.s.: not significant.

(*P* = 0.043, *f* = 0.97 and *P* < 0.001, *f* = 0.83; **Figure 9C** and **D**). To assess the involvement of GSK-3β in the effects of HSV-1 at 6TS, we inhibited this kinase by administering a lithium salt (LiCl in particular) to mice. LiCl (45 mg/kg per day) was administered via the intraperitoneal route for 3 weeks between the 5th and 6th TS. This procedure was already used to inhibit GSK-3β in a mouse model of mania (Li et al., 2023). We found that HSV-1-infected mice treated with lithium chloride exhibited a significant reduction of the pGSK-3β^{Tyr216} levels *vs.* HSV-1-infected mice in the hippocampi (0.55 ± 0.09 *vs.* 1.00 ± 0.12; *P* = 0.024, *d* = 2.79) and this effect was accompanied by a reduction of pAPP^{Thr668} (0.56 ± 0.12 *vs.* 1.00 ± 0.07; *P* = 0.018, *d* = 3.22) and pTau^{S199} (0.26 ± 0.05 *vs.* 1.00 ± 0.19; *P* = 0.020, *d* = 3.22; **Figure 9E–G**).

We then attempted to assess whether GSK-3β-dependent tau and/or APP cleavage products were responsible for the synaptic damage observed at 6TS. To this end, we applied the same infection and reactivation protocol to both APP$^{-/-}$ and Tau$^{-/-}$ mice to determine whether the absence of either protein protects against HSV-1-induced synaptic impairment. Unfortunately, both APP$^{-/-}$ and Tau$^{-/-}$ mice spontaneously develop synaptic deficits at 6–8 months of age, even in the absence of infection, making them unsuitable for addressing this specific question. Specifically, we observed impaired recognition memory in tau and APP knockout mice compared with C57BL/6 controls (PI: 56.8% ± 1.2% and 53.1% ± 2.5% *vs.* 64.9% ± 2.0% in WT mice, respectively; *P* < 0.001, *f* = 0.43 for both; **Additional Figure 7A**), accompanied by a significant reduction in LTP responses (69.9% ± 6.6%, *P* = 0.026 and 64.0% ± 6.8%, *P* = 0.022 *vs.* 103.7% ± 16.7%; *f* = 0.47; **Additional Figure 7B** and **C**).

Discussion

We recently demonstrated that neuroinflammation plays a crucial role in HSV-1-induced synaptic and cognitive dysfunction after 2TS that recapitulates some early stage of neurodegeneration (Li Puma et al., 2023). Specifically, the selective blockade of IL-1β signaling with anakinra, an IL-1R antagonist, was sufficient to prevent the functional, structural, and molecular indices of neurodegeneration in C57BL/6 WT mice that underwent two viral reactivations. Various studies link elevated pro-inflammatory mediators to cognitive decline and may accelerate the progression of neurodegenerative diseases, especially in the elderly (Leonardo and Fregni, 2023; Mekhora et al., 2024; Serna et al., 2025).

In this model of sporadic AD, we also found that 2TS not only induced a marked upregulation of IL-1β expression but also promoted the phosphorylation of GSK-3β at Tyr216 and its substrates APP and tau. Tau has gained increasing attention as a therapeutic target in AD because of its central role in pathogenic cascades (Gu and Liu, 2020; Rawat et al., 2022; Gonzalez-Ortiz et al., 2023). In particular, tau phosphorylation (e.g., at residue Ser199, T231, and S396 that are well-validated and relatively specific targets of GSK-3β) converts tau into an inhibitory, dominant-negative species that sequesters normal MAPs, reduces microtubule binding, and destabilizes microtubules, thereby impairing axonal transport and synaptic function (Alonso et al., 2004; Foidl and Humpel, 2018). Similarly, APP phosphorylation and its subsequent proteolytic cleavage generate the neurotoxic fragment Aβ and AICD, besides playing a critical role in the intercellular spreading of tau and Aβ oligomers (Multhaup et al., 2015; Puzzo et al., 2017; Li Puma et al., 2022; Puliatti et al., 2023).

Based on these observations, we sought to determine whether APP and tau also contribute to HSV-1-induced synaptic dysfunction during the early phases of neurodegeneration by using knockout mice lacking either APP or tau. Interestingly, although these animals exhibited clear cognitive deficits following 2TS, the associated impairment in LTP at CA3-CA1 synapses was significantly milder than in infected C57BL/6 mice. This partial rescue of synaptic function may be explained by the markedly lower levels of IL-1β detected in these knockout models compared with those in infected WT controls. These data suggest that the absence of APP or tau attenuates the inflammatory response, particularly by limiting the release of IL-1β. This is in line with previous reports showing that APP can act as a pro-inflammatory receptor in monocytic lineage cells, promoting the production of inflammatory mediators, including IL-1β (Sondag and Combs, 2004). Here, we demonstrated that the deletion of APP and tau, rather than directly interfering with the inflammasome, promotes the activation of alternative

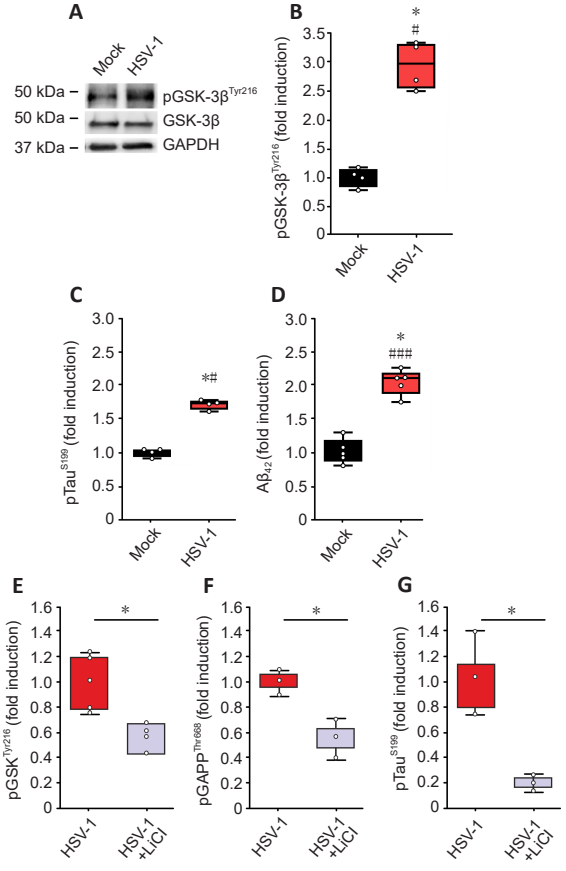

Figure 9 | GSK-3β–dependent phosphorylation of APP and tau at six cycles of thermal stress is blocked by LiCl.

(A, B) Representative western blot images (A) and densitometric analyses (B) showing increased pGSK-3β^{Tyr216} levels in mock- and HSV-1-infected mice following six cycles of thermal stress (n = 4 mice per group). GAPDH was used as a loading control. (C, D) Box plots showing mean pTau^{S199} (C) and Aβ_{42} levels measured by enzyme-linked immunosorbent assay in hippocampal homogenates from the same experimental groups described in A (n = 4/5 mice per group). (E–G) Densitometric analysis of GSK-3β–dependent phosphorylation of APP and Tau in HSV-1-infected mice treated and untreated with LiCl (n = 3/4 mice per group). Data are expressed as normalized fold changes in HSV-1-infected mice relative to mock animals. *P < 0.05, *vs.* mock; #P < 0.05, ###P < 0.005, *vs.* HSV-1 2TS group (Kruskal–Wallis one-way analysis of variance on ranks, Mann-Whitney U test, or Student's t-test). Aβ: Amyloid-β; GAPDH: glyceraldehyde 3-phosphate dehydrogenase; GSK-3β: glycogen synthase kinase 3β; HSV-1: herpes simplex virus type 1; pAPP: phosphorylated amyloid precursor protein; pGSK-3β: phosphorylated GSK-3β.

microglial pathways. In fact, in our models, NLRP3 inflammasome expression levels remained comparable across infected transgenic genotypes, indicating that IL-1β release is not the result of differential inflammasome activation but rather depends on altered microglial activation. In particular, the reduced expression of classical pro-inflammatory M1 microglial markers could explain the lower levels of the inflammatory cytokine IL-1β detected in these animals. Furthermore, RNA-seq transcriptomic analysis confirmed that HSV-1-infected WT mice exhibited marked transcriptional alterations in microglial activation-related genes, in line with previous reports in AD mouse models (Holtman et al., 2015). These alterations were absent in APP$^{-/-}$ and Tau$^{-/-}$ mice, emphasizing that the simultaneous presence of both tau and APP is required to trigger microglial activation and support the development of an AD-like phenotype. Several studies have reported that APP and/or its cleaved fragments, as well as tau, play important roles in glial cell activation and in modulating the innate immune response to CNS injury. Carrano and Das (2015) reported that in mice lacking APP, both microglial cells and astrocytes appear less reactive, showing reduced expression of glial markers as well as decreased levels of various innate immune cytokines following LPS stimulation. Consistently, Manocha et al. (2016) demonstrated that in APP$^{-/-}$ mice crossed with the APP/PS1 transgenic line, the absence of murine APP significantly reduced microgliosis despite the presence of amyloid plaques, highlighting the direct role of APP in regulating the inflammatory phenotype of microglia. Finally, more recent studies have shown that in the LPS model using CX3CR1 knockout mice, genetic ablation of tau exerts neuroprotective effects by reducing microglial activation, altering inflammatory gene expression, and decreasing the number of degenerating neurons (Maphis et al., 2015).

Next, we investigated whether inflammation remained the predominant driver of pathology at later stages of the disease. In mice undergoing 6TS, which recapitulates some late AD-like features, persistent synaptic and cognitive impairments were accompanied by a pronounced inflammatory response. However, in contrast to what was observed in the early disease stage (2TS), where IL-1R blockade was effective, anakinra treatment following 6TS failed to prevent cognitive decline, synaptic plasticity impairments, and reduction in synaptic protein expression in infected mice, indicating that mechanisms beyond IL-1β signaling contribute to pathology at later stages. Additional pro-inflammatory mediators appear to play a limited role, as dexamethasone, a broad-spectrum corticosteroid that suppresses various inflammatory genes (Patil et al., 2018), did not ameliorate HSV-1-induced synaptic dysfunction in the late stages of infection. Steroid treatment has been reported to induce HSV-1 reactivation in several experimental models (Chucair-Elliott et al., 2017; Harrison et al., 2023; Jones, 2023). However, in our study, the dexamethasone regimen employed did not induce detectable viral reactivation. Indeed, mock-infected dexamethasone-treated animals behaved similarly to untreated controls, indicating that the doses and time frame used here were insufficient to trigger HSV-1 reactivation.

We hypothesized that other molecular mechanisms, beyond neuroinflammation, might contribute to the synaptic dysfunction observed in this mouse model after 6TS. In particular, GSK-3β activation was much greater than 2TS, and it was accompanied by increased pTau at Ser199 and accumulation of the neurotoxic APP fragment Aβ. These events may exacerbate synaptic damage and help explain the ineffectiveness of anti-inflammatory treatments at this stage.

A limitation of our study was the use of constitutive knockout transgenic models, which are unsuitable for investigating whether the absence of APP or tau confers protection against HSV-1-induced synaptic impairments after 6TS. Indeed, both APP$^{-/-}$ and Tau$^{-/-}$ mice developed age-dependent synaptic deficits independently of infection. These findings are consistent with previous studies in which cognitive impairments in this mouse model have been shown to depend not only on the genetic background of the mouse, but also on the type and conditions of the behavioral or memory tests performed, as well as variations in diet and housing conditions (Lei et al., 2024). Moreover, the conflicting data reported in the literature, particularly concerning the Tau$^{-/-}$ model, may also depend on the specific Tau$^{-/-}$ line used, as at least four different knockout mouse models for the Mapt gene (which encodes the tau protein) have been generated, each with distinct genetic and phenotypic characteristics (Harada et al., 1994; Tucker et al., 2001; Fujio et al., 2007). To overcome this limitation, in future studies, we plan to perform more in-depth characterization of the role of GSK-3β activation and accumulation of hyperphosphorylated tau in HSV-1-infected mice undergone 6TS by bilateral stereotaxic intrahippocampal injections of adeno-associated viruses expressing a doxycycline-inducible short-hairpin RNA targeting tau (Velazquez et al., 2018).

Taken together, our findings underscore a complex interaction between tau/Aβ accumulation, neuroinflammation, and gene expression modulation, each contributing to impaired synaptic plasticity and memory. While proinflammatory cytokines primarily trigger neurodegenerative pathways in the early stages of the disease, GSK-3β-dependent tau/Aβ accumulation emerges as the dominant factor in later stages. This interdependence between APP/tau and neuroinflammation supports a model where both components act jointly from the beginning, with their relative contributions shifting over time.

From a translational perspective, these results highlight the importance of monitoring peripheral and cerebrospinal biomarkers related to the IL-1β and integrating them with neuroinflammatory imaging approaches, such as microglia-targeted PET (e.g., TSPO-PET), to identify optimal intervention time windows (Leng and Edison, 2021; Zhou et al., 2021; Owen et al., 2023; Rossano et al., 2024; Roveta et al., 2024; Pola et al., 2025) and the right treatment (anti-inflammatory vs anti AD molecular hallmarks – i.e., antibodies anti Aβ (Kim et al., 2025).

Acknowledgments: *We would like to acknowledge the contribution of the Core Facilities G-STeP "Electrophysiology", "Bioinformatics" and "Microscopy", Fondazione Policlinico Universitario A. Gemelli IRCCS.*

Author contributions: *Conception and design of the study, execution of western blot experiments, data analysis and interpretation, and manuscript writing: DDLP. Electrophysiological field recordings and dot blot analyses: GB. ELISA and qRT-PCR experiments and data interpretation: GP. Behavior experiments and LTP recordings: BB. Behavior experiments and data interpretation: MR. Western blot experiments: FL. Critical review of the manuscript: GDC and ATP. Conception and design of the study and manuscript writing: RP and CG. All authors finally approved the manuscript and each one is responsible for their own contribution to the work.*

Conflicts of interest: *All authors declare that they have no conflicts of interest.*

Data availability statement: *All relevant data are within the paper and its Additional files.*

Additional files:

Additional Figure 1: *Enhanced A$\beta_{40/42}$ accumulation in hippocampal neurons of HSV-1-infected mice.*

Additional Figure 2: *Synaptic and cognitive functions are similar among wild-type, APP$^{-/-}$, and Tau$^{-/-}$ mice at 4.5 months of age.*

Additional Figure 3: *HSV-1-dependent activation of the NLRP3 inflammasome.*

Additional Figure 4: *Transcriptomic profiling and Gene Ontology enrichment in mock- and HSV-1 infected C57BL/6 (A), Tau$^{-/-}$ (B), APP$^{-/-}$ mice (C).*

Additional Figure 5: *Increased IL-1β expression following six cycles of thermal stress in HSV-1-infected mice.*

Additional Figure 6: *Schematic representation of the experimental design for anakinra or dexamethasone treatment during multiple HSV-1 reactivations.*

Additional Figure 7: *altered intrinsic synaptic and cognitive functions in 8-month-old APP$^{-/-}$ and Tau$^{-/-}$ mice.*

Additional Table 1: *Summary of sample sequencing metrics.*

Additional Table 2: *Microglial gene signatures in Alzheimer's disease models.*

Additional Table 3: *Allocation of animals to experimental assays.*

Additional Table 4: *IL-1β and pGSK-3β levels in mouse cortex after 2TS (fold induction vs. mock-infected mice).*

References

Akkerman S, Prickaerts J, Steinbusch HW, Blokland A (2012) Object recognition testing: statistical considerations. Behav Brain Res 232:317-322.

Alonso Adel C, Mederlyova A, Novak M, Grundke-Iqbal I, Iqbal K (2004) Promotion of hyperphosphorylation by frontotemporal dementia tau mutations. J Biol Chem 279:34873-34881.

Araya K, Watson R, Khanipov K, Golovko G, Taglialatela G (2025) Increased risk of dementia associated with herpes simplex virus infections: Evidence from a retrospective cohort study using U.S. electronic health records. J Alzheimers Dis 104:393-402.

Ben-Aicha S, Ramos G (2025) Unravelling inflammation: the critical role of ETS2 in macrophage activation and chronic disease. Cardiovasc Res 121:833-835.

Benner C, van der Meulen T, Cacéres E, Tigyi K, Donaldson CJ, Huising MO (2014) The transcriptional landscape of mouse beta cells compared to human beta cells reveals notable species differences in long non-coding RNA and protein-coding gene expression. BMC Genomics 15:620.

Black JA, Liu S, Waxman SG (2009) Sodium channel activity modulates multiple functions in microglia. Glia 57:1072-1081.

Blevins HM, Xu Y, Biby S, Zhang S (2022) The NLRP3 inflammasome pathway: a review of mechanisms and inhibitors for the treatment of inflammatory diseases. Front Aging Neurosci 14:879021.

Bliss TV, Collingridge GL (1993) A synaptic model of memory: long-term potentiation in the hippocampus. Nature 361:31-39.

Bórquez DA, González-Billault C (2012) The amyloid precursor protein intracellular domain-fe65 multiprotein complexes: a challenge to the amyloid hypothesis for Alzheimer's disease? Int J Alzheimers Dis 2012:353145.

Carrano A, Das P (2015) Altered innate immune and glial cell responses to inflammatory stimuli in amyloid precursor protein knockout mice. PLoS One 10:e0140210.

Chen Y, Ye X, Escames G, Lei W, Zhang X, Li M, Jing T, Yao Y, Qiu Z, Wang Z, Acuña-Castroviejo D, Yang Y (2023) The NLRP3 inflammasome: contributions to inflammation-related diseases. Cell Mol Biol Lett 28:51.

Chucair-Elliott AJ, Carr MM, Carr DJJ (2017) Long-term consequences of topical dexamethasone treatment during acute corneal HSV-1 infection on the immune system. J Leukoc Biol 101:1253-1261.

Civitelli L, Marcocci ME, Celestino I, Piacentini R, Garaci E, Grassi C, De Chiara G, Palamara AT (2015) Herpes simplex virus type 1 infection in neurons leads to production and nuclear localization of APP intracellular domain (AICD): implications for Alzheimer's disease pathogenesis. J Neurovirol 21:480-90.

Colussi C, Aceto G, Ripoli C, Bertozzi A, Li Puma DD, Paccosi E, D'Ascenzo M, Grassi C (2023) Cytoplasmic HDAC4 recovers synaptic function in the 3×Tg mouse model of Alzheimer's disease. Neuropathol Appl Neurobiol 49:e12861.

De Chiara G, Marcocci ME, Civitelli L, Argnani R, Piacentini R, Ripoli C, Manservigi R, Grassi C, Garaci E, Palamara AT (2010) APP processing induced by herpes simplex virus type 1 (HSV-1) yields several APP fragments in human and rat neuronal cells. PLoS One 5:e13989.

De Chiara G, Piacentini R, Fabiani M, Mastrodonato A, Marcocci ME, Limongi D, Napoletani G, Protto V, Coluccio P, Celestino I, Li Puma DD, Grassi C, Palamara AT (2019) Recurrent herpes simplex virus-1 infection induces hallmarks of neurodegeneration and cognitive deficits in mice. PLoS Pathog 15:e1007617.

Ebrahimi R, Shahrokhi Nejad S, Falah Tafti M, Karimi Z, Sadr SR, Ramadhan Hussein D, Talebian N, Esmaeilpour K (2025) Microglial activation as a hallmark of neuroinflammation in Alzheimer's disease. Metab Brain Dis 40:207.

Foidl BM, Humpel C (2018) Differential hyperphosphorylation of Tau-S199,-T231 and-S396 in organotypic brain slices of alzheimer mice. A model to study early tau hyperphosphorylation using okadaic acid. Front Aging Neurosci 10:113.

Fujio K, Sato M, Uemura T, Sato T, Sato-Harada R, Harada A (2007) 14-3-3 proteins and protein phosphatases are not reduced in tau-deficient mice. Neuroreport 18:1049-1052.

Gan L, Ye S, Chu A, Anton K, Yi S, Vincent VA, von Schack D, Chin D, Murray J, Lohr S, Patthy L, Gonzalez-Zulueta M, Nikolich K, Urfer R (2004) Identification of cathepsin B as a mediator of neuronal death induced by Abeta-activated microglial cells using a functional genomics approach. J Biol Chem 279:5565-5572.

Gao C, Jiang J, Tan Y, Chen S (2023) Microglia in neurodegenerative diseases: mechanism and potential therapeutic targets. Signal Transduct Target Ther 8:359.

Gonzalez-Ortiz F, Kac PR, Brum WS, Zetterberg H, Blennow K, Karikari TK (2023) Plasma phospho-tau in Alzheimer's disease: towards diagnostic and therapeutic trial applications. Mol Neurodegener 18:18.

Gu JL, Liu F (2020) tau in alzheimer's disease: pathological alterations and an attractive therapeutic target. Curr Med Sci 40:1009-1021.

Hampel H, Hardy J, Blennow K, Chen C, Perry G, Kim SH, Villemagne VL, Aisen P, Vendruscolo M, Iwatsubo T, Masters CL, Cho M, Lannfelt L, Cummings JL, Vergallo A (2021) The amyloid-β pathway in Alzheimer's disease. Mol Psychiatry 26:5481-5503.

Harada A, Oguchi K, Okabe S, Kuno J, Terada S, Ohshima T, Sato-Yoshitake R, Takei Y, Noda T, Hirokawa N (1994) Altered microtubule organization in small-calibre axons of mice lacking tau protein. Nature 369:488-491.

Harrison KS, Wijesekera N, Robinson AGJ, Santos VC, Oakley RH, Cidlowski JA, Jones C (2023) Impaired glucocorticoid receptor function attenuates herpes simplex virus 1 production during explant-induced reactivation from latency in female mice. J Virol 97:e0130523.

He B, Gorijala P, Xie L, Cao S, Yan J (2022) Gene co-expression changes underlying the functional connectomic alterations in Alzheimer's disease. BMC Med Genomics 15:92.

Heneka MT, et al. (2025) Neuroinflammation in Alzheimer disease. Nat Rev Immunol 25:321-352.

Holtman IR, Raj DD, Miller JA, Schaafsma W, Yin Z, Brouwer N, Wes PD, Möller T, Orre M, Kamphuis W, Hol EM, Boddeke EW, Eggen BJ (2015) Induction of a common microglia gene expression signature by aging and neurodegenerative conditions: a co-expression meta-analysis. Acta Neuropathol Commun 3:31.

Isik S, Yeman Kiyak B, Akbayir R, Seyhali R, Arpaci T (2023) Microglia mediated neuroinflammation in Parkinson's disease. Cells 12:1012.

Jones C (2023) Intimate relationship between stress and human alpha herpes virus 1 (HSV 1) reactivation from latency. Curr Clin Microbiol Rep 10:236-245.

Joyce DA, Steer JH, Kloda A (1996) Dexamethasone antagonizes IL-4 and IL-10-induced release of IL-1RA by monocytes but augments IL-4-, IL-10-, and TGF-beta-induced suppression of TNF-alpha release. J Interferon Cytokine Res16:511-517.

Jurga AM, Paleczna M, Kuter KZ (2020) Overview of general and discriminating markers of differential microglia phenotypes. Front Cell Neurosci 14:198.

Kim BH, Kim S, Nam Y, Park YH, Shin SM, Moon M (2025) Second-generation anti-amyloid monoclonal antibodies for Alzheimer's disease: current landscape and future perspectives. Transl Neurodegener 14:6.

Lee E, Chang Y (2025) Modulating neuroinflammation as a prospective therapeutic target in Alzheimer's disease. Cells 14:168.

Lei P, Ayton S, Moon S, Zhang Q, Volitakis I, Finkelstein DI, Bush AI (2014) Motor and cognitive deficits in aged tau knockout mice in two background strains. Mol Neurodegener 9:29.

Leng F, Edison P (2021) Neuroinflammation and microglial activation in Alzheimer disease: where do we go from here? Nat Rev Neurol 17:157-172.

Leonardo S, Fregni F (2023) Association of inflammation and cognition in the elderly: A systematic review and meta-analysis. Front Aging Neurosci 15:1069439.

Li C, Zhao Z, Jin J, Zhao C, Zhao B, Liu Y (2024) nlrp3-gsdmd-dependent il-1β secretion from microglia mediates learning and memory impairment in a chronic intermittent hypoxia-induced mouse model. Neuroscience 539:51-65.

Li Puma DD, Piacentini R, Leone L, Gironi K, Marcocci ME, De Chiara G, Palamara AT, Grassi C (2019) Herpes simplex virus type-1 infection impairs adult hippocampal neurogenesis via amyloid-β protein accumulation. Stem Cells 37:1467-1480.

Li Puma DD, Ripoli C, Puliatti G, Pastore F, Lazzarino G, Tavazzi B, Arancio O, Piacentini R, Grassi C (2022) Extracellular tau oligomers affect extracellular glutamate handling by astrocytes through downregulation of GLT-1 expression and impairment of NKA1A2 function. Neuropathol Appl Neurobiol 48:e12811.

Li Puma DD, Colussi C, Bandiera B, Puliatti G, Rinaudo M, Cocco S, Paciello F, Re A, Ripoli C, De Chiara G, Bertozzi A, Palamara AT, Piacentini R, Grassi C (2023) Interleukin 1β triggers synaptic and memory deficits in Herpes simplex virus type-1-infected mice by downregulating the expression of synaptic plasticity-related genes via the epigenetic MeCP2/HDAC4 complex. Cell Mol Life Sci 80:172.

Li R, Liu W, Yin J, Chen Y, Guo S, Fan H, Li X, Zhang X, He X, Duan C (2018) TSG-6 attenuates inflammation-induced brain injury via modulation of microglial polarization in SAH rats through the SOCS3/STAT3 pathway. J Neuroinflammation 15:231.

Li X, Chen B, Zhang D, Wang S, Feng Y, Wu X, Cui L, Ji M, Gong W, Verkhratsky A, Xia M, Li B (2023) A novel murine model of mania. Mol Psychiatry 28:3044-3054.

Liang T, Zhang Y, Wu S, Chen Q, Wang L (2022) The Role of NLRP3 Inflammasome in Alzheimer's disease and potential therapeutic targets. Front Pharmacol 13:845185.

Liu Y, Johnston C, Jarousse N, Fletcher SP, Iqbal S (2025) Association between herpes simplex virus type 1 and the risk of Alzheimer's disease: a retrospective case-control study. BMJ Open 15:e093946.

Lövheim H, Gilthorpe J, Johansson A, Eriksson S, Hallmans G, Elgh F (2015) Herpes simplex infection and the risk of Alzheimer's disease: A nested case-control study. Alzheimers Dement 11:587-92.

Manocha GD, Floden AM, Rausch K, Kulas JA, McGregor BA, Rojanathammanee L, Puig KR, Puig KL, Karki S, Nichols MR, Darland DC, Porter JE, Combs CK (2016) APP regulates microglial phenotype in a mouse model of Alzheimer's disease. J Neurosci 36:8471-86.

Maphis N, Xu G, Kokiko-Cochran ON, Cardona AE, Ransohoff RM, Lamb BT, Bhaskar K (2015) Loss of tau rescues inflammation-mediated neurodegeneration. Front Neurosci 9:196.

Mekhora C, Lamport DJ, Spencer JPE (2024) An overview of the relationship between inflammation and cognitive function in humans, molecular pathways and the impact of nutraceuticals. Neurochem Int 181:105900.

Miller JA, Horvath S, Geschwind DH (2010) Divergence of human and mouse brain transcriptome highlights Alzheimer disease pathways. Proc Natl Acad Sci U S A 107:12698-12703.

Multhaup G, Huber O, Buée L, Galas MC (2015) Amyloid precursor protein (APP) metabolites APP intracellular fragment (AICD), Aβ42, and Tau in nuclear roles. J Biol Chem 290:23515-23522.

Ng LL, Chow J, Lau KF (2024) The AICD interactome: implications in neurodevelopment and neurodegeneration. Biochem Soc Trans 52:2539-2556.

Owen M, Bose N, Nisenbaum L, Partrick KA, Fillit HM (2023) The critical role of biomarkers for drug development targeting the biology of aging. J Prev Alzheimers Dis 10:729-742.

Patil RH, Naveen Kumar M, Kiran Kumar KM, Nagesh R, Kavya K, Babu RL, Ramesh GT, Chidananda Sharma S (2018) Dexamethasone inhibits inflammatory response via down regulation of AP-1 transcription factor in human lung epithelial cells. Gene 645:85-94.

Piacentini R, Li Puma DD, Ripoli C, Marcocci ME, De Chiara G, Garaci E, Palamara AT, Grassi C (2015) Herpes simplex virus type-1 infection induces synaptic dysfunction in cultured cortical neurons via GSK-3 activation and intraneuronal amyloid-β protein accumulation. Sci Rep 5:15444.

Pola I, Ashton NJ, Antônio De Bastiani M, Brum WS, Rahmouni N, Tan K, Machado LS, Servaes S, Stevenson J, Tissot C, Therriault J, Pascoal TA, Blennow K, Zetterberg H, Zimmer ER, Rosa-Neto P, Benedet AL (2025) Exploring inflammation-related protein expression and its relationship with TSPO PET in Alzheimer's disease. Alzheimers Dement 21:e70171.

Pradeepkiran JA, Baig J, Islam MA, Kshirsagar S, Reddy PH (2024) Amyloid-beta and phosphorylated tau are the key biomarkers and predictors of Alzheimer's disease. Aging Dis 16:658-682.

Puliatti G, Li Puma DD, Aceto G, Lazzarino G, Acquarone E, Mangione R, D'Adamio L, Ripoli C, Arancio O, Piacentini R, Grassi C (2023) Intracellular accumulation of tau oligomers in astrocytes and their synaptotoxic action rely on amyloid precursor protein intracellular domain-dependent expression of glypican-4. Prog Neurobiol 227:102482.

Puzzo D, Piacentini R, Fá M, Gulisano W, Li Puma DD, Staniszewski A, Zhang H, Tropea MR, Cocco S, Palmeri A, Fraser P, D'Adamio L, Grassi C, Arancio O (2017) LTP and memory impairment caused by extracellular Aβ and Tau oligomers is APP-dependent. Elife 6:e26991.

Rawat P, Sehar U, Bisht J, Selman A, Culberson J, Reddy PH (2022) Phosphorylated Tau in Alzheimer's disease and other tauopathies. Int J Mol Sci 23:12841.

Rossano SM, Johnson AS, Smith A, Ziaggi G, Roetman A, Guzman D, Okafor A, Klein J, Tomljanovic Z, Stern Y, Brickman AM, Lee S, Kreisl WC, Lao P (2024) Microglia measured by TSPO PET are associated with Alzheimer's disease pathology and mediate key steps in a disease progression model. Alzheimers Dement 20:2397-2407.

Roveta F, Bonino L, Piella EM, Rainero I, Rubino E (2024) Neuroinflammatory biomarkers in Alzheimer's disease: from pathophysiology to clinical implications. Int J Mol Sci 25:11941.

Selkoe DJ (2002) Alzheimer's disease is a synaptic failure. Science 298:789-91.

Serna MF, Mosquera M, García-Perdomo HA (2025) Inflammatory markers and their relationship with cognitive function in Alzheimer's disease and mild cognitive impairment. Systematic review and meta-analysis. Neuromolecular Med 27:53.

Shishkina GT, Kalinina TS, Lanshakov DA, Bulygina VV, Komysheva NP, Bannova AV, Drozd US, Dygalo NN (2023) Genes involved by dexamethasone in prevention of long-term memory impairment caused by lipopolysaccharide-induced neuroinflammation. Biomedicines 11:2595.

Smedley D, Haider S, Ballester B, Holland R, London D, Thorisson G, Kasprzyk A (2009) BioMart--biological queries made easy. BMC Genomics 10:22.

Sondag CM, Combs CK (2004) Amyloid precursor protein mediates proinflammatory activation of monocytic lineage cells. J Biol Chem 279:14456-14463.

Spires-Jones TL, Hyman BT (2014) The intersection of amyloid beta and tau at synapses in Alzheimer's disease. Neuron 82:756-771.

Strickland BA, Ansari SA, Dantoft W, Uhlenhaut NH (2022) How to tame your genes: mechanisms of inflammatory gene repression by glucocorticoids. FEBS Lett 596:2596-2616.

Sudwarts A, Thinakaran G (2023) Alzheimer's genes in microglia: a risk worth investigating. Mol Neurodegener 18:90.

Sun N, Victor MB, Park YP, Xiong X, Scannail AN, Leary N, Prosper S, Viswanathan S, Luna X, Boix CA, James BT, Tanigawa Y, Galani K, Mathys H, Jiang X, Ng AP, Bennett DA, Tsai LH, Kellis M (2023) Human microglial state dynamics in Alzheimer's disease progression. Cell 186:4386-4403.e29.

Tucker KL, Meyer M, Barde YA (2001) Neurotrophins are required for nerve growth during development. Nat Neurosci 4:29-37.

Udeochu JC, et al. (2023) Tau activation of microglial cGAS-IFN reduces MEF2C-mediated cognitive resilience. Nat Neurosci 26:737-750.

Valiukas Z, Tangalakis K, Apostolopoulos V, Feehan J (2025) Microglial activation states and their implications for Alzheimer's disease. J Prev Alzheimers Dis 12:100013.

Velazquez R, Ferreira E, Tran A, Turner EC, Belfiore R, Branca C, Oddo S (2018) Acute tau knockdown in the hippocampus of adult mice causes learning and memory deficits. Aging Cell 17:e12775.

Vestin E, Boström G, Olsson J, Elgh F, Lind L, Kilander L, Lövheim H, Weidung B (2024) Herpes simplex viral infection doubles the risk of dementia in a contemporary cohort of older adults: A prospective study. J Alzheimers Dis 97:1841-1850.

Wickham H (2016) ggplot2: Elegant Graphics for Data Analysis. Springer Nature Link.

Xu S, Hu E, Cai Y, Xie Z, Luo X, Zhan L, Tang W, Wang Q, Liu B, Wang R, Xie W, Wu T, Xie L, Yu G (2024) Using clusterProfiler to characterize multiomics data. Nat Protoc 19:3292-3320.

Xu YJ, Au NPB, Ma CHE (2022) Functional and phenotypic diversity of microglia: Implication for microglia-based therapies for Alzheimer's disease. Front Aging Neurosci 14:896852.

Yang X, et al. (2023) Functional characterization of Alzheimer's disease genetic variants in microglia. Nat Genet 55:1735-1744.

Ye Q, Lin B, Xu P, Zhang F, Wang N, Shou D (2024) Yunvjian decoction attenuates lipopolysaccharide-induced periodontitis by suppressing NFκB/NLRP3/IL-1β pathway. J Ethnopharmacol 319:117279.

Yu H, Xiong M, Zhang Z (2023) The role of glycogen synthase kinase 3 beta in neurodegenerative diseases. Front Mol Neurosci 16:1209703.

Zhang W, Xiao D, Mao Q, Xia H (2023) Role of neuroinflammation in neurodegeneration development. Signal Transduct Target Ther 8:267.

Zhou Q, Li S, Li M, Ke D, Wang Q, Yang Y, Liu GP, Wang XC, Liu E, Wang JZ (2022) Human tau accumulation promotes glycogen synthase kinase-3β acetylation and thus upregulates the kinase: A vicious cycle in Alzheimer neurodegeneration. EbioMedicine 78:103970.

Zhou R, Ji B, Kong Y, Qin L, Ren W, Guan Y, Ni R (2021) PET imaging of neuroinflammation in Alzheimer's disease. Front Immunol 12:739130.

Editors: LCH, SLP, ZM, ZLJ